Interactions and chemical reactions in ionic alkali-metal and alkaline-earth-metal diatomic AB^+ and triatomic A_2B^+ systems

Michał Śmiałkowski [1,2] and Michał Tomza [1,*]
[1] *Faculty of Physics, University of Warsaw, Pasteura 5, 02-093 Warsaw, Poland*
[2] *Faculty of Chemistry, University of Warsaw, Pasteura 1, 02-093 Warsaw, Poland*

(Received 29 October 2019; published 6 January 2020)

We theoretically characterize interactions, energetics, and chemical reaction paths in ionic two-body and three-body systems of alkali-metal and alkaline-earth-metal atoms in the context of modern experiments with cold hybrid ion-atom mixtures. Using *ab initio* techniques of quantum chemistry such as the coupled-cluster method, we calculate ground-state electronic properties of all diatomic AB^+ and most of the triatomic A_2B^+ molecular ions consisting of Li, Na, K, Rb, Cs, Mg, Ca, Sr, Ba, and Yb atoms. Different geometries and wave-function symmetries of the ground state are found for different classes of molecular ions. We analyze intermolecular interactions in the investigated systems including additive two-body and nonadditive three-body ones. As an example we provide two-dimensional interaction potential-energy surfaces for $KRb^+ + K$ and $Rb^+ + Sr_2$ mixtures. We identify possible channels of chemical reactions based on the energetics of the reactants. The present results may be useful for investigating controlled chemical reactions and other applications of molecular ions formed in cold hybrid ion-atom systems.

DOI: 10.1103/PhysRevA.101.012501

I. INTRODUCTION

The field of ultracold quantum matter has seen groundbreaking developments in recent years, unfolding perspectives for numerous applications in precision measurements [1], many-body physics [2], and controlled chemistry [3] experiments. Laser cooling and trapping techniques have allowed one to prepare and manipulate ultracold atoms, ions, and molecules with full control over their quantum states, recently, also at the single-particle level [4,5]. Further developments in experimental methods have opened the way for combining ultracold trapped ions and atoms in a single experimental setup [6–8]. Most of the ion-atom experiments use alkaline-earth-metal ions trapped and laser cooled in a Paul trap immersed into ultracold neutral alkali-metal or alkaline-earth-metal atoms trapped in magnetic, magneto-optical, or dipole traps [8]. Alkaline-earth-metal ions and alkali-metal atoms are employed because of their electronic structure favorable for laser cooling. Several cold atomic ion-atom combinations have already been experimentally investigated, including $Yb^+ + Yb$ [9], $Ca^+ + Rb$ [10], $Ba^+ + Ca$ [11], $Yb^+ + Ca$ [12], $Yb^+ + Rb$ [13], $Ca^+ + Li$ [14], $Ca^+ + Rb$ [15], $Ca^+ + Na$ [16], $Yb^+ + Li$ [17,18], $Sr^+ + Rb$ [19], $Rb^+ + Rb$ [20,21], and $Na^+ + Na$ [22].

Cold hybrid ion-atom experiments can be used to realize and investigate cold collisions [13,20,23], controlled chemical reactions [24,25], charge-transfer and spin-transfer dynamics [18,26], quantum simulation [27], and quantum computation [28]. In such systems, diatomic molecular ions can be produced via spontaneous or stimulated charge-transfer radiative association or photoassociation [29,30]; however, only $RbCa^+$ [10,15], $RbBa^+$ [31], $CaYb^+$ [12], and $CaBa^+$ [11] molecular ions have been observed as products of cold collisions between respective ions and atoms. For higher atomic densities, the three-body processes resulting in the formation of molecular ions additionally play a role [21,32,33]. Cold molecular ions can also be produced by the ionization of ultracold molecules [34–36] or by sympathetic cooling of molecular ions from higher temperature [37,38]. Molecular ions, which possess additional rotational and vibrational degrees of freedom, can likewise be immersed into ultracold atomic gases opening the way for novel applications in cold controlled ion-atom chemistry [39–46], precision measurement [47,48], and quantum simulation of many-body physics [49]. In this context, we investigate theoretically the two-body and three-body interactions and chemical reactions in ionic alkali-metal and alkaline-earth-metal diatomic and triatomic systems.

Three-body and many-body nonadditive interactions are important for understanding the emergence of bulk matter properties, crucial across all areas of physics [50]. They have been theoretically investigated in neutral spin-polarized triatomic molecules consisting of alkali-metal atoms [51–56], alkali-earth-metal atoms [53,57,58], and Cu, Zn, Au, and Ag atoms [53,59,60]. The nonadditive interactions have also been intensely studied in clusters of ions with small molecules [61,62]. In contrast, the knowledge of nonadditive interactions in metallic molecular ions or ionic clusters is limited [63–70].

In this paper, we theoretically investigate the ground-state electronic structure of single-charged molecular ions formed from two or three interacting alkali-metal and alkaline-earth-metal atoms. We calculate ground-state electronic properties of all diatomic AB^+ and most of the triatomic A_2B^+ molecular

*michal.tomza@fuw.edu.pl

 ©2020 American Physical Society

ions consisting of Li, Na, K, Rb, Cs, Mg, Ca, Sr, Ba, and Yb atoms using *ab initio* techniques of quantum chemistry. We obtain equilibrium distances, atomization energies, ionization potentials, permanent electric dipole moments, and polarizabilities. A variety of equilibrium geometries for the trimers from linear through isosceles triangular to equilateral triangular are discovered. Furthermore, we evaluate and characterize three-body nonadditive interactions in these systems at equilibrium geometries. We also provide two-dimensional interaction potential-energy surfaces for exemplary nonreactive $KRb^+ + K$ and $Sr_2 + Rb^+$ mixtures. We identify possible channels of chemical reactions in ionic two-body $A^+ + B$ and AB^+ and three-body $A^+ + AB$, $AB^+ + A$, and A_2B^+ systems, based on the energetics of the reactants. Additionally, we present example calculations of minimum-energy paths for the isomerization reaction of linear alkali-metal trimers in the lowest triplet electronic state between asymmetric AAB^+ and symmetric ABA^+ arrangements. The present results may be useful for investigating controlled chemical reactions and other applications of molecular ions in modern experiments with cold ion-atom mixtures.

The paper has the following structure. Section II describes the theoretical methods used in the *ab initio* electronic structure calculations. Section III presents and discusses the results concerning diatomic molecular ions, triatomic molecular ions, and channels of chemical reactions. Section IV summarizes the paper and points to further applications and extensions of the presented results and methodology.

II. THEORETICAL METHODS

In order to obtain potential-energy curves (PECs) and surfaces (PESs) within the Born-Oppenheimer approximation, we adopt the computational scheme successfully applied to the ground-state interactions between polar alkali-metal dimers [56] and between linear polyatomic anions with alkali-metal and alkaline-earth-metal atoms [43]. Thus, to calculate PECs and PESs we employ the close-shell or spin-restricted open-shell coupled cluster methods restricted to single, double, and noniterative triple excitations, starting from the restricted closed-shell or open-shell Hartree-Fock orbitals, CCSD(T) [71,72]. The interaction energies are obtained with the supermolecule method and the basis set superposition error is corrected by using the counterpoise correction [73]

$$\begin{aligned} V_{AB} &= E_{AB} - E_A - E_B, \\ V_{ABC} &= E_{ABC} - E_A - E_B - E_C, \\ V_{AB+C} &= E_{ABC} - E_{AB} - E_C, \end{aligned} \tag{1}$$

where V_{AB}, V_{ABC}, and V_{AB+C} are interaction energies between A and B; A, B, and C; and AB within the rigid rotor approximation and C, respectively. E_{ABC}, E_{AB}, and E_X denote the total energy of trimer, dimer, and monomer computed in a dimer or trimer basis set.

The three-body nonadditive interatomic interaction in triatomic molecular ions is defined as

$$V_{3b} = V_{ABC} - V_{AB} - V_{BC} - V_{AC}, \tag{2}$$

where V_{ABC} is the interaction energy in the three-atom system while V_{XY} are the two-body interactions, all defined by Eq. (1) and calculated in the trimer basis set. The effective three-body interatomic interaction emerges as a many-electron quantum effect despite the fact that only the genuine two-body Coulomb interactions between electrons and nuclei are present in the underlying electronic Hamiltonian.

The Li, Na, and Mg atoms are described with the augmented correlation-consistent polarized core-valence quadruple-ζ quality basis sets (aug-cc-pCVQZ) [74]. The scalar relativistic effects in the K, Rb, Cs, Ca, Sr, Ba, and Yb atoms are included by employing the small-core relativistic energy-consistent pseudopotentials (ECPs) to replace the inner-shell electrons [75]. The use of the pseudopotentials allows one to model the inner-shell electron density as accurately as the high quality atomic calculations employed to fit the pseudopotentials and to use larger basis sets to describe the valence electrons. The pseudopotentials from the Stuttgart library are used in the presented calculations. The K, Ca, Rb, Sr, Cs, Ba, and Yb atoms are described with the ECP10MDF, ECP10MDF, ECP28MDF, ECP28MDF, ECP46MDF, ECP46MDF, and ECP60MDF pseudopotentials [76,77] and the $[11s11p5d3f]$, $[12s12p7d4f2g]$, $[14s14p7d6f1g]$, $[14s11p6d5f4g]$, $[12s11p6d4f2g]$, $[13s12p6d5f4g]$, and $[10s10p9d5f3g]$ basis sets, respectively, obtained by decontracting and augmenting the basis sets suggested in Refs. [76,77]. The used basis sets were developed in Refs. [78–81]. The basis sets are additionally augmented in all calculations for diatomic molecular ions by the set of the $[3s3p2d2f1g]$ bond functions [82].

To find equilibrium interatomic distances for diatomic molecular ions AB^+, we calculate full PECs, whereas for triatomic molecular ions A_2B^+ we explore two-dimensional PESs around their minima. To this end, we employ two kinds of a PES minimization. First, and for the majority of systems, we assume an isoscales triangular geometry with each of the A atoms bound to the B atom situated on the symmetry axis of the molecular ion. Therefore the PES becomes a two-dimensional function of two coordinates $V(R, \theta)$, where R is the distance between the B atom and each of the A atoms, and θ is the angle between the two legs of the triangle. When θ equals 180°, the molecular ion becomes linear and shows a higher symmetry of the $D_{\infty h}$ point group with the general formula ABA^+. The second kind of the PES minimization applies to linear trimers that fall into the $C_{\infty v}$ symmetry group with the general formula AAB^+. Then, the PES is a function of two interatomic distances $V(R_{AA}, R_{AB})$, where R_{AA} is the distance between two A atoms, and R_{AB} is the distance between the central A atom and B atom. We confirm that found minima are not saddle points in three-dimensional optimizations.

The static electric dipole and quadrupole polarizabilities of atoms and the polarizabilities and permanent electric dipole moments of diatomic molecular ions are calculated with the CCSD(T) and finite field methods. The z axis is chosen along the internuclear axis and is oriented from an atom with a larger ionization potential to an atom with a smaller ionization potential, and the origin is set in the center of mass. The adiabatic and vertical ionization potentials (IP_{ad} and IP_{ver}) and the vertical electron attachment energies (EA_{ver}) are extracted

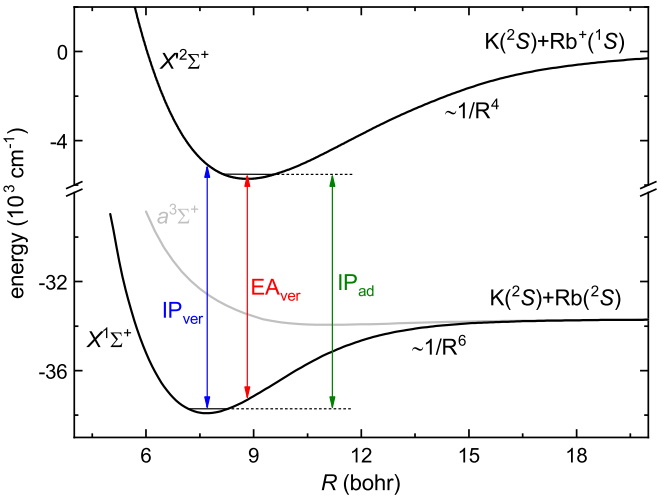

FIG. 1. Ground-state potential-energy curves for the KRb molecule and KRb^+ molecular ions together with definitions of the adiabatic and vertical ionization potentials (IP_{ad} and IP_{ver}), and the vertical electron attachment energy (EA_{ver}).

from energy calculations for diatomic molecular ions AB^+ and neutral molecules AB as presented for the exemplary KRb^+ molecular ion in Fig. 1.

To assess the accuracy of the employed *ab initio* methods, Table I collects the static electric dipole and quadrupole polarizabilities, ionization potentials, and the lowest $S-P$ excitation energies of alkali-metal and alkaline-earth-metal atoms. Present theoretical values are compared with the most accurate available theoretical or experimental data. The calculated static electric dipole and quadrupole polarizabilities agree with previous data within 0.1–5.7 and 9–314 a.u. that correspond to an error of 0.1–2.2 and 0.6–3.7%, respectively. The ionization potentials and the lowest $S-P$ excitation energies coincide with experimental results within 23–255 and 7–190 cm^{-1} that is 0.05–0.6 and 0.05–1%, respectively. Additionally, we compare the available experimental data for the $^1\Sigma^+$ state of all 15 neutral alkali-metal molecules [91] with calculated values, and the mean absolute error for the dissociation energy is 74 cm^{-1} (1.6%), while for the equilibrium bound length it is 0.013 bohr (0.18%). Overall agreement between calculated properties and the most accurate available theoretical or experimental data is very good. This confirms that the employed CCSD(T) method, energy-consistent pseudopotentials, and basis sets properly reproduce correlation energy and include relativistic effects, while being close to convergence in the size of the basis function set. Thus, the used methodology should also provide an accurate description of interaction energies for investigated molecular ions. Based on the above and our previous experience, we estimate the total uncertainty of the calculated PECs for diatomic molecular ions and PESs for triatomic molecular ions at the global minima to be of the order of 100–300 cm^{-1} that corresponds to 2–5% of the interaction energy. Larger uncertainty may be expected in systems with larger number of valence electrons. The lack of the exact treatment of the triple and higher excitations in the employed CCSD(T) method and the quality of employed energy-consistent pseudopotentials in reproduction of relativistic effects are primary limiting factors.

All electronic structure calculations are performed with the MOLPRO package of *ab initio* programs [93]. The isosurfaces of electronic density for selected trimers are generated with the Gaussian software [94].

TABLE I. Characteristics of alkali-metal and alkaline-earth-metal atoms: the static electric dipole polarizability α, the static electric quadrupole polarizability β, the ionization potential IP, and the lowest $S-P$ excitation energy ($^2S-{}^2P$ for alkali-metal atoms and $^1S-{}^3P$ for alkaline-earth-metal atoms). Present theoretical values are compared with the most accurate available theoretical or experimental data.

Atom	α (a.u.)	β (a.u.)	IP (cm^{-1})	$S-P$ (cm^{-1})
Li	164.3	1414	43464	14911
	164.2 [83]	1423 [84]	43487 [85]	14904 [85]
Na	166.4	1920	41217	16799
	162.7 [86]	1895 [87]	41449 [85]	16968 [85]
K	290.8	4970	34949	13022
	290.0 [88]	4947 [87]	35010 [85]	13024 [85]
Rb	319.5	6578	33566	12686
	320.1 [88]	6491 [87]	33691 [85]	12737 [85]
Cs	395.5	10343	31331	11594
	401.2 [88]	10470 [89]	31406 [85]	11548 [85]
Mg	71.8	821	61466	21701
	71.3 [90]	812 [90]	61671 [85]	21891 [85]
Ca	156.9	2946	49243	15190
	157.1 [90]	3081 [90]	49306 [85]	15263 [85]
Sr	199.2	4551	45814	14639
	197.2 [90]	4630 [90]	45932 [85]	14705 [85]
Ba	276.8	8586	41780	13106
	273.5 [90]	8900 [90]	42035 [85]	13099 [85]
Yb	143.5	2642	50267	17635
	141.0 [92]	2560 [92]	50443 [85]	18903 [85]

III. RESULTS AND DISCUSSION

A. Diatomic molecular ions AB^+

The electronic ground state of diatomic molecular ions AB^+ composed of either two alkali-metal or two alkaline-earth-metal atoms is of an open-shell doublet $^2\Sigma^+$ symmetry, which becomes $^2\Sigma_g^+$ for homonuclear alkali-metal ions and $^2\Sigma_u^+$ for homonuclear alkaline-earth-metal ions. Diatomic molecular ions containing one alkali-metal atom and one alkaline-earth-metal atom have a closed-shell singlet $^1\Sigma^+$ symmetry. All considered diatomic molecular ions, with the exception of $LiBa^+$, are described well by single-reference wave functions at all internuclear distances. The closed-shell $LiBa^+$ molecular ion dissociates into two open-shell atoms.

The electronic structures of diatomic molecular ions have previously been studied for several atomic combinations, including Li_2^+ [36,95–99], Na_2^+ [100,101], K_2^+ [102–107], Rb_2^+ [108,109], Cs_2^+ [109,110], $LiNa^+$ [111–114], LiK^+ [115–117], $LiRb^+$ [118], $LiCs^+$ [119,120], NaK^+ [117,121], $NaRb^+$ [122], $NaCs^+$ [119,123], KRb^+ [124], KCs^+ [125], $RbCs^+$ [109,126], Mg_2^+ [127,128], Ca_2^+ [127,129], $CaBa^+$ [11], $CaYb^+$ [12], Sr_2^+ [127], Ba_2^+ [127], Yb_2^+

TABLE II. Characteristics of alkali-metal diatomic molecular ions in the $^2\Sigma^+$ electronic ground state: equilibrium interatomic distance R_e (in bohr), well depth D_e (in cm^{-1}), harmonic constant ω_e (in cm^{-1}), rotational constant B_e (in cm^{-1}), permanent electric dipole moment d_e (in D), perpendicular and parallel components of the static electric dipole polarizability $\alpha_e^{\parallel}$ and $\alpha_e^{\perp}$ (in a.u.), vertical electron attachment energy $\mathrm{EA_{ver}}$ (in cm^{-1}), vertical and adiabatic ionization potential of corresponding neutral molecule $\mathrm{IP_{ver}}$ (in cm^{-1}) and $\mathrm{IP_{ad}}$ (in cm^{-1}), and dissociation limit. Previous calculations are cited in the last column.

AB^+	R_e	D_e	ω_e	B_e	d_e	$\alpha_e^{\parallel}$	$\alpha_e^{\perp}$	$\mathrm{EA_{ver}}$	$\mathrm{IP_{ver}}$	$\mathrm{IP_{ad}}$	Diss.	Previous
Li_2^+	5.85	10451	263	0.500	0	54.4	61.3	40662	42392	41521	$Li^+ + Li$	[36,95–99]
$LiNa^+$	6.36	8047	192	0.277	−3.76	88.8	72.1	39623	41377	40474	$Na^+ + Li$	[111–114]
LiK^+	7.28	4822	154	0.191	−3.59	120	96.1	35537	37169	36346	$K^+ + Li$	[115–117]
$LiRb^+$	7.61	4146	139	0.160	−4.69	136	103	34621	36234	35431	$Rb^+ + Li$	[118]
$LiCs^+$	8.07	3478	126	0.140	−4.75	156	114	32893	34544	33736	$Cs^+ + Li$	[119,120]
Na_2^+	6.81	7961	120	0.113	0	136	82.2	38640	40375	39466	$Na^+ + Na$	[100,101]
NaK^+	7.69	4644	91.6	0.0704	0.20	176	107	34806	36361	35565	$K^+ + Na$	[117,121]
$NaRb^+$	8.01	3972	77.2	0.0519	−2.35	194	114	33928	35456	34682	$Rb^+ + Na$	[122]
$NaCs^+$	8.44	3226	68.5	0.0431	−2.93	209	124	32299	33768	33046	$Cs^+ + Na$	[119,123]
K_2^+	8.52	6625	72.7	0.0426	0	265	150	32115	33416	32742	$K^+ + K$	[102–107]
KRb^+	8.81	5728	60.0	0.0290	−3.38	303	161	31488	32748	32092	$Rb^+ + K$	[124]
KCs^+	9.24	4626	53.5	0.0234	−4.24	335	179	30167	31361	30746	$Cs^+ + K$	[125]
Rb_2^+	9.10	6151	46.0	0.0171	0	347	173	30863	32074	31443	$Rb^+ + Rb$	[108,109]
$RbCs^+$	9.53	4952	39.8	0.0128	−1.19	391	193	29637	30887	30185	$Cs^+ + Rb$	[109,126]
Cs_2^+	9.95	5796	34.0	0.00915	0	452	217	28630	29699	29140	$Cs^+ + Cs$	[109,110]

[130], $LiMg^+$[131,132], KMg^+ [133], $LiCa^+$[132,134,135], $NaCa^+$ [136–138], $RbCa^+$ [30,139], $LiSr^+$ [140,141], $NaSr^+$ [140,142,143], KSr^+ [140,144], $RbSr^+$ [30,140], $CsSr^+$ [140], $RbBa^+$ [30,145,146], $LiYb^+$ [29,30], and $RbYb^+$ [30,147,148].

Here, for completeness and comparison, and to analyze trends, we calculate the electronic ground-state properties of all 55 diatomic molecular ions consisting of Li, Na, K, Rb, Cs, Mg, Ca, Sr, Ba, and Yb atoms. Among investigated homo- and heteronuclear molecular ions, 15 species consist of two alkali-metal atoms, 15 species consist of two alkaline-earth-metal atoms, and 25 species consist of one alkali-metal atom and one alkaline-earth-metal atom. The calculated properties include ground-state potential-energy curves, equilibrium interatomic distances R_e, well depths D_e, harmonic constants ω_e, rotational constants B_e, permanent electric dipole moments d_e, perpendicular and parallel components of the static electric dipole polarizabilities $\alpha_e^{\parallel}$ and $\alpha_e^{\perp}$, vertical electron attachment energies EA, and vertical and adiabatic ionization potentials of corresponding neutral molecules $\mathrm{IP_{ver}}$ and $\mathrm{IP_{ad}}$. They are collected in Table II for alkali-metal molecular ions, in Table III for alkaline-earth-metal molecular ions, and in Table IV for mixed alkali-metal–alkaline-earth-metal molecular ions. To calculate harmonic and rotational constants, atomic masses of the most abundant isotopes are assumed. Additionally PECs and permanent electric dipole moments for selected systems are presented in Figs. 2 and 3, respectively. Full potential-energy curves, permanent electric dipole moments, and electric dipole polarizabilities as a function of interatomic distance are available for all investigated systems from the authors upon request.

Ion-atom interactions are dominated by the induction component, which can be understood in terms of the interaction of the charge of an ion with the electronic cloud of a neutral partner [8]. Therefore, PECs for all investigated diatomic molecular ions have the average of the well depths around $6000\,\mathrm{cm}^{-1}$ and are deeper than PECs for corresponding neutral molecules. Among alkali-metal dimers, the Li_2^+ molecular ion is the most strongly bound with $D_e = 10\,451\,\mathrm{cm}^{-1}$, while the $NaCs^+$ molecular ion is the most weakly bound with $D_e = 3226\,\mathrm{cm}^{-1}$. Among alkaline-earth-metal dimers, the Mg_2^+ molecular ion is the most strongly bound with $D_e = 10\,532\,\mathrm{cm}^{-1}$, while the $MgBa^+$ molecular ion is the most weakly bound with $D_e = 3569\,\mathrm{cm}^{-1}$. Among mixed alkali-metal–alkaline-earth-metal dimers the range of binding energies is the largest. For this class of compounds, the $LiBa^+$ molecular ion is the most strongly bound with $D_e = 11\,674\,\mathrm{cm}^{-1}$, while the $CsMg^+$ molecular ion is the most weakly bound with $D_e = 1861\,\mathrm{cm}^{-1}$. For all considered groups of molecular ions, larger binding energies are mostly correlated with smaller equilibrium distances. All equilibrium interatomic distances are between 5.45 bohrs for $LiMg^+$ and 9.95 bohrs for Cs_2^+ with the average around 7.5 bohrs.

In general, all homonuclear diatomic molecular ions are more strongly bound than related heteronuclear ones due to the more efficient charge delocalization in homonuclear ions. Within homonuclear compounds, the lightest elements have the largest binding energies [see Figs. 2(a) and 2(d)]. If the charge is localized at one of the atoms (the one with a smaller ionization potential), then the strength of the interaction is correlated with the polarizability of the neutral partner [see Figs. 2(b) and 2(c) where the charge is mostly localized at Rb, especially at larger internuclear distances, except $RbCs^+$]. Within mixed alkali-metal–alkaline-earth-metal molecular ions, with the exception of $LiBa^+$, the positive charge is localized at the alkali-metal atom due to its much lower ionization potential (electronegativity) (see Table I). Thus, in the series of molecular ions consisting of the Rb

TABLE III. Characteristics of alkaline-earth-metal diatomic molecular ions in the $^2\Sigma^+$ electronic ground state: equilibrium interatomic distance R_e (in bohr), well depth D_e (in cm^{-1}), harmonic constant ω_e (in cm^{-1}), rotational constant B_e (in cm^{-1}), permanent electric dipole moment d_e (in D), perpendicular and parallel components of the static electric dipole polarizability $\alpha_e^{\parallel}$ and $\alpha_e^{\perp}$ (in a.u.), vertical electron attachment energy EA_{ver} (in cm^{-1}), vertical and adiabatic ionization potential of corresponding neutral molecule IP_{ver} (in cm^{-1}) and IP_{ad} (in cm^{-1}), and dissociation limit. Previous calculations are cited in the last column.

AB^+	R_e	D_e	ω_e	B_e	d_e	$\alpha_e^{\parallel}$	$\alpha_e^{\perp}$	EA_{ver}	IP_{ver}	IP_{ad}	Diss.	Previous
Mg_2^+	5.70	10532	215	0.154	0	143	75.7	50233	54898	51503	$Mg^+ + Mg$	[127,128]
$MgCa^+$	6.53	5334	153	0.0941	−0.51	239	122	43887	45769	44549	$Ca^+ + Mg$	
$MgSr^+$	6.92	4216	122	0.0667	−1.37	253	141	41770	43234	42312	$Sr^+ + Mg$	
$MgBa^+$	7.30	3569	107	0.0553	−2.06	269	178	38722	39784	39139	$Ba^+ + Mg$	
$MgYb^+$	6.88	4280	118	0.0603	−3.35	209	106	45481	48268	46482	$Yb^+ + Mg$	
Ca_2^+	7.23	9285	130	0.0576	0	293	167	40425	41880	40935	$Ca^+ + Ca$	[127,129]
$CaSr^+$	7.58	7273	105	0.0381	−2.42	372	186	39115	40440	39594	$Sr^+ + Ca$	
$CaBa^+$	7.97	5946	91.4	0.0306	−3.42	412	228	36795	37745	37161	$Ba^+ + Ca$	[11]
$CaYb^+$	7.46	7585	98.7	0.0333	6.07	315	155	41124	44287	42180	$Ca^+ + Yb$	[12]
Sr_2^+	7.92	8575	80.2	0.0218	0	366	210	37849	39137	38310	$Sr^+ + Sr$	[127]
$SrBa^+$	8.29	6825	68.6	0.0163	−1.16	460	250	35911	36940	36299	$Ba^+ + Sr$	
$SrYb^+$	7.82	5920	68.2	0.0168	4.75	341	178	39535	42234	40486	$Sr^+ + Yb$	
Ba_2^+	8.67	8596	59.8	0.0116	0	476	290	34362	35207	34690	$Ba^+ + Ba$	[127]
$BaYb^+$	8.21	4826	54.8	0.0116	3.90	355	220	36874	39124	37726	$Ba^+ + Yb$	
Yb_2^+	7.76	7089	56.8	0.0115	0	330	142	42410	46143	43645	$Yb^+ + Yb$	[130]

TABLE IV. Characteristics of alkali-metal–alkaline-earth-metal diatomic molecular ions in the $^1\Sigma^+$ electronic ground state: equilibrium interatomic distance R_e (in bohr), well depth D_e (in cm^{-1}), harmonic constant ω_e (in cm^{-1}), rotational constant B_e (in cm^{-1}), permanent electric dipole moment d_e (in D), perpendicular and parallel components of the static electric dipole polarizability $\alpha_e^{\parallel}$ and $\alpha_e^{\perp}$ (in a.u.), vertical electron attachment energy EA_{ver} (in cm^{-1}), vertical and adiabatic ionization potential of corresponding neutral molecule IP_{ver} (in cm^{-1}) and IP_{ad} (in cm^{-1}), and dissociation limit. Previous calculations are cited in the last column.

AB^+	R_e	D_e	ω_e	B_e	d_e	$\alpha_e^{\parallel}$	$\alpha_e^{\perp}$	EA_{ver}	IP_{ver}	IP_{ad}	Diss.	Previous
$LiMg^+$	5.48	6628	266	0.369	5.45	75.9	56.0	38159	38483	38291	$Li^+ + Mg$	[131,132]
$LiCa^+$	6.16	9941	246	0.266	4.54	156	105	35844	35985	35911	$Li^+ + Ca$	[132,134,135]
$LiSr^+$	6.45	11126	230	0.223	5.04	196	124	34619	34786	34699	$Li^+ + Sr$	[140,141]
$LiBa^+$	6.71	11674	225	0.200	−4.06	271	147	33407	33472	33435	$Ba^+ + Li$	
$LiYb^+$	6.29	8719	225	0.225	7.28	139	92.2	34848	36781	35569	$Li^+ + Yb$	[29,30]
$NaMg^+$	6.09	4517	151	0.138	3.20	88.3	60.2	37590	38038	37755	$Na^+ + Mg$	
$NaCa^+$	6.70	7336	137	0.0918	2.54	182	114	35542	35701	35604	$Na^+ + Ca$	[136–138]
$NaSr^+$	6.97	8418	121	0.0680	4.34	226	135	34446	34668	34533	$Na^+ + Sr$	[140,142,143]
$NaBa^+$	7.24	10318	115	0.0582	3.93	307	164	33110	33220	33169	$Na^+ + Ba$	
$NaYb^+$	6.82	6386	114	0.0637	7.75	167	100	34877	36927	35591	$Na^+ + Yb$	
KMg^+	7.07	2614	102	0.0811	3.24	92.9	66.8	32917	33242	33045	$K^+ + Mg$	[133]
KCa^+	7.71	4281	93.2	0.0513	3.37	192	129	31794	31946	31854	$K^+ + Ca$	
KSr^+	7.99	4950	79.5	0.0350	6.27	241	156	31104	31326	31191	$K^+ + Sr$	[140,144]
KBa^+	8.30	6170	75.8	0.0288	6.69	325	197	30211	30333	30259	$K^+ + Ba$	
KYb^+	7.81	3688	71.4	0.0310	10.3	176	113	31192	32674	31759	$K^+ + Yb$	
$RbMg^+$	7.41	2237	84.1	0.0586	0.78	99.2	70.4	31933	32227	32051	$Rb^+ + Mg$	
$RbCa^+$	8.06	3666	73.9	0.0341	0.39	202	134	30997	31140	31054	$Rb^+ + Ca$	[30,139]
$RbSr^+$	8.34	4247	59.0	0.0201	3.41	253	162	30397	30608	30479	$Rb^+ + Sr$	[30,140]
$RbBa^+$	8.65	5314	54.3	0.0153	4.33	339	206	29611	29737	29661	$Rb^+ + Ba$	[30,145,146]
$RbYb^+$	8.15	3152	49.6	0.0159	8.41	184	118	30436	31745	30949	$Rb^+ + Yb$	[147,148]
$CsMg^+$	7.85	1861	73.2	0.0481	−0.03	109	76.6	30022	30262	30122	$Cs^+ + Mg$	
$CsCa^+$	8.53	3017	63.2	0.0270	−0.63	213	141	29336	29448	29382	$Cs^+ + Ca$	
$CsSr^+$	8.81	3484	48.7	0.0147	2.16	264	170	28850	29023	28919	$Cs^+ + Sr$	[140]
$CsBa^+$	9.14	4350	44.0	0.0106	3.28	351	217	28228	28341	28273	$Cs^+ + Ba$	
$CsYb^+$	8.61	2591	39.3	0.0108	7.37	194	125	28755	29867	29213	$Cs^+ + Yb$	

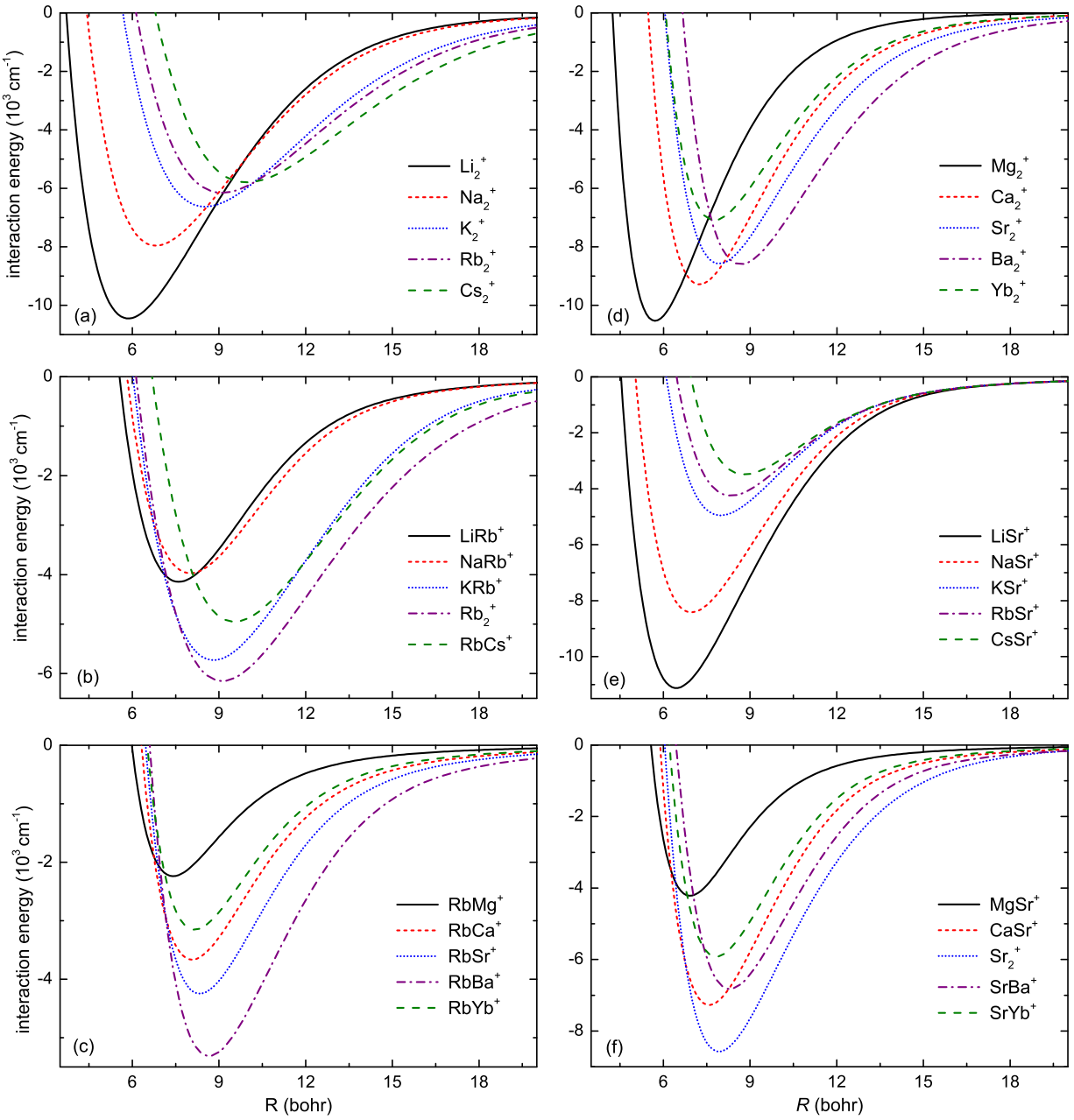

FIG. 2. Ground-state potential-energy curves for selected diatomic molecular ions: (a) homonuclear alkali-metal dimers, (b) heteronuclear alkali-metal dimers containing Rb atoms, (c) heteronuclear alkali-metal–alkaline-earth-metal dimers containing Rb atoms, (d) homonuclear alkaline-earth-metal dimers, (e) heteronuclear alkali-metal–alkaline-earth-metal dimers containing Sr atoms, and (f) heteronuclear alkaline-earth-metal dimers containing Sr atoms.

ion and alkaline-earth-metal atom, the dissociation energy increases visibly with increasing polarizability of the alkaline-earth-metal atom and is the largest for the $RbBa^+$ molecular ion while the lowest for the $RbMg^+$ one [see Fig. 2(c)]. In contrast, in the series of molecular ions consisting of the Sr atom and alkali-metal ion, the long-range part of the interaction is determined by the polarizability of the Sr atom and is similar for all compounds. Additionally, a clear trend of an increasing binding energy with the decreasing atomic size is visible for those molecular ions, that indicates a certain degree of covalent bonding [see Fig. 2(e)].

The permanent electric dipole moments are calculated with respect to the center of mass, which is a natural choice for studying the rovibrational dynamics. Exemplary results for selected diatomic molecular ions are presented in Fig. 3. Their absolute values increase with increasing internuclear distance and asymptotically approach the limiting cases $d(R) \approx \frac{\mu}{m_{A^+}} R$, where the charge is completely localized on the ion A^+ corresponding to the atom with the smaller ionization potential (m_{A^+} is the mass of the A^+ ion and μ is the reduced mass of the ion-atom system). This behavior is typical for heteronuclear molecular ions and implies that even molecular ions in very

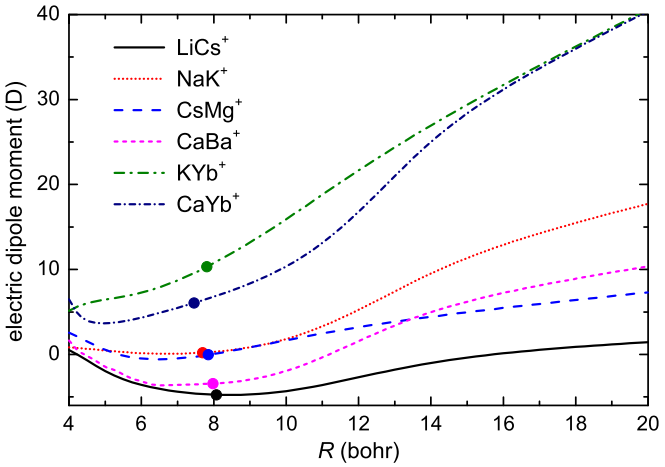

FIG. 3. Permanent electric dipole moments for selected diatomic molecular ions. The z axis is oriented from the atom with a larger ionization potential to the atom with a smaller ionization potential and the origin is in the center of mass. The points indicate values for equilibrium distances.

weakly bound states have effectively a significant permanent electric dipole moment in contrast to neutral molecules [149]. The differences between calculated values and limiting cases are the interaction-induced variations of the permanent electric dipole moments or, in other words, they describe the degree of charge transfer and delocalization. For most of the alkali-metal and alkaline-earth-metal dimers, the calculated permanent dipole moments have a negative sign for the equilibrium distance. This means that the charge is significantly delocalized and transferred from the ion with smaller ionization potential to the second atom due to chemical bonding and orbital mixing at equilibrium distances. For alkali-metal–alkaline-earth-metal molecular ions, the sign of the permanent dipole moments is mostly positive, indicating weaker charge transfer and delocalization. In general, the calculated permanent electric dipole moments take values between zero and 10 D for KYb^+. Large permanent electric dipole moments may be useful for control with electromagnetic fields or dipolar interactions. Similarly, calculated molecular polarizabilities describe interactions with the laser field and may give information about anisotropy of intermolecular interactions [150].

The ionization potentials for all molecular ions AB^+ are smaller than the smallest ionization potential among related constituent atoms A and B, because PECs for molecular ions AB^+ are deeper than for neutral molecules AB (see Fig. 1). At the same time the adiabatic and vertical ionization potentials of neutral molecules AB and the vertical electron attachment energies to molecular ions AB^+ are very similar, because the equilibrium distances for molecular ions and parent neutral molecules are similar.

Calculated PECs' parameters agree well with results obtained previously for selected systems by other authors, including spectroscopic measurements and calculations using different electronic structure methods such as effective large-core pseudopotentials with core-polarization potentials. Absolute deviations of potentials' well depths between previous results and our results in most cases are in the range of 100–300 cm^{-1}, within our estimated error bars (see, e.g., Refs. [30,98,108,118,136,139–141,146–148] for representative examples). The equilibrium distances agree within 0.05–0.2 bohr. Calculations with large-core pseudopotentials [30,109,134,138,140,141,143,144] have a tendency to give smaller equilibrium distances but the overall agreement between calculations with small-core and large-core pseudopotentials is good and cross validates both approaches. For the readability of calculated characteristics collected in Tables II–IV and due to space limitations, we do not present detailed comparison of all existing calculations for diatomic molecular ions with our calculations but cite them. Detailed comparison is presented in Supplemental Material [151].

B. Triatomic molecular ions A_2B^+

Assuming an isosceles triangular geometry, triatomic heteronuclear molecular ions A_2B^+ composed of three alkali-metal atoms in the electronic ground state have a closed-shell $^1A_1$ symmetry within the C_{2v} point group. Homonuclear trimers A_3^+ of alkali-metal atoms additionally show threefold rotational symmetry. The lowest energetic triplet state of the alkali-metal trimers has a $^3B_2$ symmetry. The ground state of alkaline-earth-metal trimers has a doublet multiplicity and can be either in a $^2A_1$ or $^2B_2$ representation of the C_{2v} symmetry group. Homonuclear alkaline-earth-metal trimers do not show threefold symmetry as opposed to homonuclear alkali-metal triatomic ions.

We calculate the potential-energy surfaces for all 25 alkali-metal triatomic molecular ions A_2B^+ consisting of Li, Na, K, Rb, and Cs in the lowest singlet $^1A_1$ electronic state (ground state) at the isosceles triangular geometry and all 45 alkali-metal triatomic molecular ions in the lowest triplet $^3B_2$ electronic state which coreduces to the $^3\Sigma_u^+$ and $^3\Sigma^+$ symmetries at two possible linear geometries ABA^+ and AAB^+, respectively. The equilibrium geometries, that is, the equilibrium angles between the two even legs of the triangle α_e, the equilibrium leg lengths R_{AB} for the isosceles triangular singlet states, the equilibrium distances between the first and the second atom R_{12}, and the equilibrium distances between the second and the third atom R_{23} for the linear triplet states, are collected in Tables V and VI, respectively.

We also calculate the potential-energy surfaces for 20 symmetric forms of alkaline-earth-metal triatomic molecular ions ABA^+ consisting of Mg, Ca, Sr, Ba, and Yb in the lowest doublet $^2A_1$ electronic state at the isosceles triangular geometry and 16 asymmetric forms of alkaline-earth-metal triatomic molecular ions AAB^+ in the doublet $^2A_1$ electronic ground state which coreduces to the $^3\Sigma^+$ symmetry at the linear geometry. Additionally, we investigate the potential-energy surfaces for 20 symmetric alkaline-earth-metal triatomic molecular ions A_2B^+ in the lowest doublet $^2B_2$ electronic state at the isosceles triangular geometry. Their equilibrium geometries are reported in Tables VII, VIII, and IX, respectively. Combinations containing more than one Yb atom are not presented because of numerical complexity and discrepancies between results obtained with different pseudopotentials.

Together with equilibrium geometries, the well depths of the triatomic ions and their decomposition into additive

TABLE V. Characteristics of alkali-metal triatomic molecular ions A_2B^+ in the singlet $^1A_1$ electronic ground state. All molecular ions have an isosceles triangular equilibrium geometry within the C_{2v} point group. Consecutive columns list: equilibrium angle between the two even legs of the triangle α_e, equilibrium leg length R_{AB}, well depth of the triatomic ion D_e, additive two-body part of the binding energy D_{2b}, nonadditive three-body part of the binding energy D_{3b}, and dissociation limit.

A_2B^+	α_e (degree)	R_{AB} (bohr)	D_e (cm^{-1})	D_{2b} (cm^{-1})	D_{3b} (cm^{-1})	Diss.
Li_3^+	60.0	5.62	23610	28799	−5190	$Li^+ + Li + Li$
Li_2Na^+	53.8	6.14	20281	24119	−3838	$Na^+ + Li + Li$
Li_2K^+	43.6	7.21	15583	17975	−2391	$K^+ + Li + Li$
Li_2Rb^+	41.1	7.58	14607	16666	−2059	$Rb^+ + Li + Li$
Li_2Cs^+	38.0	8.08	13514	15371	−1857	$Cs^+ + Li + Li$
Na_2Li^+	65.7	6.08	26004	22534	3470	$Na^+ + Na + Li$
Na_3^+	60.0	6.53	18317	21318	−3001	$Na^+ + Na + Na$
Na_2K^+	48.7	7.58	13435	15070	−1636	$K^+ + Na + Na$
Na_2Rb^+	46.1	7.92	12417	13771	−1354	$Rb^+ + Na + Na$
Na_2Cs^+	42.4	8.45	11240	12344	−1104	$Cs^+ + Na + Na$
K_2Li^+	82.7	6.79	15305	17111	−1806	$K^+ + K + Li$
K_2Na^+	75.6	7.19	14263	16037	−1773	$K^+ + K + Na$
K_3^+	60.0	8.25	14425	17153	−2728	$K^+ + K + K$
K_2Rb^+	56.5	8.60	13147	15468	−2321	$Rb^+ + K + K$
K_2Cs^+	52.0	9.13	11495	13394	−1898	$Cs^+ + K + K$
Rb_2Li^+	89.1	7.05	14389	15588	−1199	$Rb^+ + Rb + Li$
Rb_2Na^+	81.0	7.44	13318	14665	−1347	$Rb^+ + Rb + Na$
Rb_2K^+	63.8	8.49	13217	15617	−2400	$Rb^+ + Rb + K$
Rb_3^+	60.0	8.85	13258	15779	−2521	$Rb^+ + Rb + Rb$
Rb_2Cs^+	54.6	9.39	11502	13574	−2072	$Cs^+ + Rb + Rb$
Cs_2Li^+	101.2	7.39	13793	14167	−373	$Cs^+ + Cs + Li$
Cs_2Na^+	91.0	7.76	12590	13202	−612	$Cs^+ + Cs + Na$
Cs_2K^+	70.4	8.81	11937	14047	−2110	$Cs^+ + Cs + K$
Cs_2Rb^+	66.0	9.17	11868	14143	−2275	$Cs^+ + Cs + Rb$
Cs_3^+	60.0	9.73	12118	14733	−2615	$Cs^+ + Cs + Cs$

two-body and nonadditive three-body parts are reported in Tables V–IX. The full potential well depth equals to the sum of all two-body and three-body contributions. The three-body nonadditive part, depending on its sign, may both stabilize and destabilize molecular ions. For molecular ions, and ion-neutral complexes in general, there is an ambiguity in the decomposition of the interaction energy into two-body or many-body contributions, because this decomposition depends on the formal assignment of the charge to one of the monomers. In the interacting ion-neutral systems, the charge can be delocalized or transferred to another monomer. The problem is minimized for systems where one of the monomers has significantly smaller ionization potential than others. In the present paper, we assume that the charge is associated with the atom with the smallest ionization potential. For homonuclear molecular ions the most symmetric position of the charge is assumed. The interplay of the two-body and three-body interactions in the investigated molecular ions is discussed in the following paragraphs.

All heteronuclear alkali-metal triatomic molecular ions A_2B^+ have the electronic ground state of the singlet $^1A_1$ symmetry at an isosceles triangular geometry with the B on the symmetry axis within the C_{2v} point group (see Table V). Homonuclear ions A_3^+ have the electronic ground state of the singlet $^1A'_1$ symmetry at an equilateral triangular geometry within the D_{3h} point group. The Na_2Li^+ molecular ion is the most strongly bound with $D_e = 26\,004\,\text{cm}^{-1}$, followed by Li_3^+ and Li_2Na^+ with $D_e = 23\,610$ and $20\,281\text{cm}^{-1}$, respectively. The Na_2Cs^+, K_2Cs^+, and Rb_2Cs^+ molecular ions are the most weakly bound with $D_e = 11\,240$, $11\,495$, and $11\,502\,\text{cm}^{-1}$, respectively. Interestingly, the three-body interaction destabilizes all alkali-metal triatomic molecular ions except for the most strongly bound Na_2Li^+, which is stabilized by $D_{3b} = 3470\,\text{cm}^{-1}$. On the other hand, the Li_3^+ molecular ion with the largest stabilizing two-body term has also the largest destabilizing three-body term of $D_{3b} = -5190\,\text{cm}^{-1}$. The present predictions of equilibrium geometries agree with previous works on alkali-metal triatomic molecular ions [63–67,69,70,152], while previously predicted well depths are usually underestimated probably because they were obtained using smaller basis sets and lower level methods.

Equilibrium internuclear distances between any two of the three atoms in singlet-state alkali-metal triatomic molecular ions are generally smaller than in the corresponding ionic and neutral dimers. The shortening is typically around 0.1–0.3 bohr, with the average of 0.25 bohr for homonuclear ions, and the largest values of 0.68 bohr for Cs_2Na^+ and Cs_2Li^+. The largest shortening is observed for systems with

TABLE VI. Characteristics of alkali-metal triatomic molecular ions AAB^+ and ABA^+ in the lowest triplet $^3B_2$ electronic state which coreduces to the $^3\Sigma^+$ and $^3\Sigma_u^+$ symmetries at a linear equilibrium geometry within the $C_{\infty v}$ and $D_{\infty h}$ point groups, respectively. Consecutive columns list: equilibrium distance between the first and the second atom R_{12}, equilibrium distance between the second and the third atom R_{23}, well depth of the triatomic ion D_e, additive two-body part of the binding energy D_{2b}, nonadditive three-body part of the binding energy D_{3b}, and dissociation limit.

ABC^+	R_{12} (bohr)	R_{23} (bohr)	D_e (cm^{-1})	D_{2b} (cm^{-1})	D_{3b} (cm^{-1})	Diss.
$LiLiLi^+$	5.90	5.90	16856	21014	−4158	$Li^+ + Li + Li$
$LiNaLi^+$	6.54	6.54	12843	16117	−3274	$Na^+ + Li + Li$
$LiLiNa^+$	5.95	6.43	14173	9331	4842	$Na^+ + Li + Li$
$LiKLi^+$	7.46	7.46	8146	9644	−1498	$K^+ + Li + Li$
$LiLiK^+$	6.02	7.29	9669	5402	4267	$K^+ + Li + Li$
$LiRbLi^+$	7.80	7.80	7033	8282	−1249	$Rb^+ + Li + Li$
$LiLiRb^+$	6.05	7.59	8650	4644	4006	$Rb^+ + Li + Li$
$LiCsLi^+$	8.25	8.25	5836	6947	−1111	$Cs^+ + Li + Li$
$LiLiCs^+$	6.09	8.01	7409	3926	3483	$Cs^+ + Li + Li$
$NaLiNa^+$	6.44	6.44	13712	9608	4104	$Na^+ + Na + Li$
$NaNaLi^+$	6.98	6.56	12539	8481	4058	$Na^+ + Na + Li$
$NaNaNa^+$	6.99	6.99	12270	15938	−3668	$Na^+ + Na + Na$
$NaKNa^+$	7.86	7.86	7742	9292	−1550	$K^+ + Na + Na$
$NaNaK^+$	7.13	7.78	7770	4843	2927	$K^+ + Na + Na$
$NaRbNa^+$	8.19	8.19	6677	12856	−6179	$Rb^+ + Na + Na$
$NaNaRb^+$	7.18	8.07	6794	4109	2686	$Rb^+ + Na + Na$
$NaCsNa^+$	8.63	8.63	5512	6443	−932	$Cs^+ + Na + Na$
$NaNaCs^+$	7.28	8.47	5600	3290	2310	$Cs^+ + Na + Na$
$KLiK^+$	7.35	7.35	10657	6732	3925	$K^+ + K + Li$
$KKLi^+$	8.63	7.56	9288	6843	2445	$K^+ + K + Li$
$KNaK^+$	7.88	7.88	9151	5876	3275	$K^+ + K + Na$
$KKNa^+$	8.63	7.96	9096	6663	2433	$K^+ + K + Na$
KKK^+	8.72	8.72	10169	13256	−3087	$K^+ + K + K$
$KRbK^+$	9.03	9.03	8917	11451	−2533	$Rb^+ + K + K$
$KKRb^+$	8.74	8.98	9066	6139	2927	$Rb^+ + K + K$
$KCsK^+$	9.47	9.47	7377	9242	−1864	$Cs^+ + K + K$
$KKCs^+$	8.80	9.37	7520	4933	2587	$Cs^+ + K + K$
$RbLiRb^+$	7.66	7.66	9818	6001	3817	$Rb^+ + Rb + Li$
$RbRbLi^+$	9.23	7.94	8350	6349	2001	$Rb^+ + Rb + Li$
$RbNaRb^+$	8.19	8.19	8346	5198	3148	$Rb^+ + Rb + Na$
$RbRbNa^+$	9.23	8.33	8186	6182	2004	$Rb^+ + Rb + Na$
$RbKRb^+$	9.01	9.01	9299	6500	2799	$Rb^+ + Rb + K$
$RbRbK^+$	9.30	9.06	9140	6471	2669	$Rb^+ + Rb + K$
$RbRbRb^+$	9.33	9.33	9342	12300	−2957	$Rb^+ + Rb + Rb$
$RbCsRb^+$	9.77	9.77	7744	9892	−2148	$Cs^+ + Rb + Rb$
$RbRbCs^+$	9.39	9.71	7725	5251	2474	$Cs^+ + Rb + Rb$
$CsLiCs^+$	8.09	8.09	9114	5475	3639	$Cs^+ + Cs + Li$
$CsCsLi^+$	10.09	8.43	7518	6036	1482	$Cs^+ + Cs + Li$
$CsNaCs^+$	8.63	8.63	7589	4599	2990	$Cs^+ + Cs + Na$
$CsCsNa^+$	10.08	8.83	7378	5867	1511	$Cs^+ + Cs + Na$
$CsKCs^+$	9.45	9.45	8292	5531	2761	$Cs^+ + Cs + K$
$CsCsK^+$	10.14	9.56	8101	6039	2062	$Cs^+ + Cs + K$
$CsRbCs^+$	9.77	9.77	8259	5698	2561	$Cs^+ + Cs + Rb$
$CsCsRb^+$	10.16	9.82	8257	6061	2196	$Cs^+ + Cs + Rb$
$CsCsCs^+$	10.22	10.22	8685	11576	−2891	$Cs^+ + Cs + Cs$

TABLE VII. Characteristics of symmetric forms of alkaline-earth-metal triatomic molecular ions ABA^+ in the lowest doublet $^2A_1$ electronic state within the C_{2v} point group which coreduces to the $^3\Sigma_g^+$ symmetry at a linear equilibrium geometry within the $D_{\infty h}$ point group. Calculated potential-energy surfaces for most of the molecular ions have two local minima: one at the linear or obtuse angle isosceles triangular geometry (below both listed as linear) and another at the acute angle isosceles triangular geometry (below listed as triangular). Characteristics for both minima are included. Consecutive columns list: equilibrium angle between the two even legs of the triangle α_e, equilibrium leg length R_{AB}, well depth of the triatomic ion D_e, additive two-body part of the binding energy D_{2b}, nonadditive three-body part of the binding energy D_{3b}, and dissociation limit.

A_2B^+	Geometry	α_e (degree)	R_{AB} (bohr)	D_e (cm^{-1})	D_{2b} (cm^{-1})	D_{3b} (cm^{-1})	Diss.
Mg_3^+	Linear	180.0	5.76	16408	21127	−4720	$Mg^+ + Mg + Mg$
Mg_2Ca^+	Linear	180.0	6.63	9200	10677	−1477	$Ca^+ + Mg + Mg$
Mg_2Sr^+	Linear	140.6	7.02	7418	8444	−1026	$Sr^+ + Mg + Mg$
Mg_2Sr^+	Triangular	65.2	6.85	7564	8781	−1218	$Sr^+ + Mg + Mg$
Mg_2Ba^+	Linear	169.3	7.41	6386	7130	−744	$Ba^+ + Mg + Mg$
Mg_2Ba^+	Triangular	58.8	7.00	7114	7237	−123	$Ba^+ + Mg + Mg$
Mg_2Yb^+	Linear	144.8	7.04	7169	8535	−1367	$Yb^+ + Mg + Mg$
Ca_2Mg^+	Linear	180.0	6.51	12201	6857	5344	$Ca^+ + Ca + Mg$
Ca_3^+	Linear	180.0	7.34	14599	18611	−4012	$Ca^+ + Ca + Ca$
Ca_3^+	Triangular	79.0	7.14	13874	19326	−5452	$Sr^+ + Ca + Ca$
Ca_2Sr^+	Linear	180.0	7.72	11909	14544	−2635	$Sr^+ + Ca + Ca$
Ca_2Sr^+	Triangular	69.4	7.42	11826	15371	−3546	$Sr^+ + Ca + Ca$
Ca_2Ba^+	Linear	146.5	8.13	9933	11890	−1957	$Ba^+ + Ca + Ca$
Ca_2Ba^+	Triangular	62.1	7.67	11091	12546	−1454	$Ba^+ + Ca + Ca$
Ca_2Yb^+	Linear	180.0	7.69	11493	7899	3594	$Ca^+ + Ca + Yb$
Sr_2Mg^+	Linear	180.0	6.86	10978	5898	5079	$Sr^+ + Sr + Mg$
Sr_2Ca^+	Linear	180.0	7.68	12962	8729	4233	$Sr^+ + Sr + Ca$
Sr_2Ca^+	Triangular	79.6	7.40	12218	14354	−2136	$Sr^+ + Sr + Ca$
Sr_3^+	Linear	167.9	8.08	13311	17160	−3850	$Sr^+ + Sr + Sr$
Sr_3^+	Triangular	74.4	7.74	13184	17982	−4798	$Sr^+ + Sr + Sr$
Sr_2Ba^+	Linear	148.1	8.47	11158	13643	−2485	$Ba^+ + Sr + Sr$
Sr_2Ba^+	Triangular	63.9	8.03	12208	14375	−2167	$Ba^+ + Sr + Sr$
Sr_2Yb^+	Linear	180.0	8.04	9919	6382	3536	$Sr^+ + Sr + Yb$
Ba_2Mg^+	Linear	180.0	7.19	10737	5755	4982	$Ba^+ + Ba + Mg$
Ba_2Mg^+	Triangular	95.7	6.84	9442	10051	−609	$Ba^+ + Ba + Mg$
Ba_2Ca^+	Linear	180.0	8.02	12085	7828	4257	$Ba^+ + Ba + Ca$
Ba_2Ca^+	Triangular	78.8	7.59	11916	13798	−1882	$Ba^+ + Ba + Ca$
Ba_2Sr^+	Linear	180.0	8.43	12174	8473	3701	$Ba^+ + Ba + Sr$
Ba_2Sr^+	Triangular	73.2	7.96	12395	14993	−2599	$Ba^+ + Ba + Sr$
Ba_3^+	Linear	158.3	8.85	13319	17195	−3876	$Ba^+ + Ba + Ba$
Ba_3^+	Triangular	65.5	8.26	14938	17911	−2973	$Ba^+ + Ba + Ba$
Ba_2Yb^+	Linear	180.0	8.42	8958	5574	3384	$Ba^+ + Ba + Yb$
Ba_2Yb^+	Triangular	77.6	8.11	8279	11531	−3251	$Ba^+ + Ba + Yb$

the smallest destabilizing effect of the three-body interaction. Equilibrium angles $\measuredangle ABA^+$ range from 38° for Li_2Cs^+ to 101° for Cs_2Li^+ and correlate with the size of involved atoms, i.e., they are acute when $m_A < m_B$ and obtuse when $m_A > m_B$.

All heteronuclear alkali-metal triatomic molecular ions in the lowest triplet electronic state have two linear equilibrium geometries: symmetric ABA^+ and asymmetric AAB^+ ones, separated by an energy barrier of a few thousand cm^{-1} (see Table VI). The symmetry of the electronic wave function for the symmetric equilibrium is $^3\Sigma_u^+$ while it is $^3\Sigma^+$ for the asymmetric one. The LiLiLi+ molecular ion is the most strongly bound with $D_e = 16\,856\,cm^{-1}$, while the $NaCsNa^+$ molecular ion is the most weakly bound with $D_e = 5512\,cm^{-1}$. If the ionization potential of A is larger than that of B, then the asymmetric AAB^+ equilibrium geometry has a smaller energy, otherwise the symmetric ABA^+ geometry is a global minimum of the triplet potential-energy surface. Interestingly, the three-body interaction destabilizes all triplet-state homonuclear alkali-metal triatomic molecular ions (e.g., Li_3^+ by $D_{3b} = -4158\,cm^{-1}$), whereas its effect for heteronuclear ABA^+ and AAB^+ ions depends on the ionization potentials of A and B atoms. If the ionization potential of A is smaller than that of B, then the three-body interaction stabilizes both

TABLE VIII. Characteristics of asymmetric forms of alkaline-earth-metal triatomic molecular ions AAB^+ in the lowest doublet $^2A_1$ electronic state which coreduces to the $^2\Sigma^+$ symmetry at a linear equilibrium geometry within the $C_{\infty v}$ point group. Consecutive columns list: equilibrium distance between the first and the second atom R_{12}, equilibrium distance between the second and the third atom R_{23}, well depth of the triatomic ion D_e, additive two-body part of the binding energy D_{2b}, nonadditive three-body part of the binding energy D_{3b}, and dissociation limit.

AAB^+	R_{12} (bohr)	R_{23} (bohr)	D_e (cm^{-1})	D_{2b} (cm^{-1})	D_{3b} (cm^{-1})	Diss.
$MgMgCa^+$	5.98	6.45	8946	5436	3510	$Ca^+ + Mg + Mg$
$MgMgSr^+$	6.05	6.80	7253	4353	2900	$Sr^+ + Mg + Mg$
$MgMgBa^+$	6.13	7.13	6238	3744	2493	$Ba^+ + Mg + Mg$
$MgMgYb^+$	5.87	6.82	7904	4146	3758	$Yb^+ + Mg + Mg$
$CaCaMg^+$	7.24	6.78	12038	9765	2274	$Ca^+ + Ca + Mg$
$CaCaSr^+$	7.54	7.48	11819	8470	3349	$Sr^+ + Ca + Ca$
$CaCaBa^+$	7.49	7.94	9936	7054	2882	$Ba^+ + Ca + Ca$
$CaCaYb^+$	7.26	7.77	12901	9584	3317	$Ca^+ + Ca + Yb$
$SrSrMg^+$	7.94	7.23	10678	9115	1563	$Sr^+ + Sr + Mg$
$SrSrCa^+$	8.45	7.76	12518	9287	3231	$Sr^+ + Sr + Ca$
$SrSrBa^+$	8.19	8.36	10956	7970	2986	$Ba^+ + Sr + Sr$
$SrSrYb^+$	7.95	8.25	11257	8906	2351	$Sr^+ + Sr + Yb$
$BaBaMg^+$	8.74	7.62	10373	9238	1135	$Ba^+ + Ba + Mg$
$BaBaCa^+$	8.78	8.25	11811	9775	2036	$Ba^+ + Ba + Ca$
$BaBaSr^+$	8.80	8.55	12327	9789	2538	$Ba^+ + Ba + Sr$
$BaBaYb^+$	8.89	8.97	10676	9080	1595	$Ba^+ + Ba + Yb$

ABA^+ and AAB^+ ions, otherwise the three-body interaction stabilizes asymmetric AAB^+ ions but destabilizes symmetric ABA^+ ones. The largest stabilizing three-body energy term of $D_{3b} = 4842\,cm^{-1}$ is for the asymmetric $LiLiNa^+$ molecular ion, while the largest destabilizing three-body energy term of $D_{3b} = -6179\,cm^{-1}$ is for the symmetric $NaRbNa^+$ molecular ion. Equilibrium internuclear distances between any two of the three atoms in triplet-state alkali-metal triatomic molecular ions are generally larger than in the corresponding ionic dimers.

TABLE IX. Characteristics of alkaline-earth-metal triatomic molecular ions A_2B^+ in the lowest doublet $^2B_2$ electronic state. All molecular ions have an isosceles triangular equilibrium geometry within the C_{2v} point group. Consecutive columns list: equilibrium angle between the two even legs of the triangle α_e, equilibrium leg length R_{AB}, well depth of the triatomic ion D_e, additive two-body part of the binding energy D_{2b}, nonadditive three-body part of the binding energy D_{3b}, and dissociation limit.

A_2B^+	α_e (degree)	R_{AB} (bohr)	D_e (cm^{-1})	D_{2b} (cm^{-1})	D_{3b} (cm^{-1})	Diss.
Mg_3^+	42.3	7.47	13604	17861	−4257	$Mg^+ + Mg + Mg$
Mg_2Ca^+	43.2	7.30	3964	7482	−3518	$Ca^+ + Mg + Mg$
Mg_2Sr^+	40.3	7.70	1883	5177	−3294	$Sr^+ + Mg + Mg$
Mg_2Yb^+	40.1	7.87	4314	5212	−898	$Yb^+ + Mg + Mg$
Ca_2Mg^+	59.0	7.03	11939	14586	−2647	$Ca^+ + Ca + Mg$
Ca_3^+	51.5	7.90	13662	18727	−5065	$Ca^+ + Ca + Ca$
Ca_2Sr^+	49.6	8.16	11149	13510	−2361	$Sr^+ + Ca + Ca$
Ca_2Ba^+	47.4	8.43	8075	10984	−2909	$Ba^+ + Ca + Ca$
Ca_2Yb^+	49.3	8.34	12399	16329	−3930	$Ca^+ + Ca + Yb$
Sr_2Mg^+	61.1	7.44	11176	12848	−1672	$Sr^+ + Sr + Mg$
Sr_2Ca^+	58.9	7.55	12808	15905	−3097	$Sr^+ + Sr + Ca$
Sr_3^+	54.4	8.32	13064	17673	−4609	$Sr^+ + Sr + Sr$
Sr_2Ba^+	49.9	8.85	10087	12824	−2737	$Ba^+ + Sr + Sr$
Sr_2Yb^+	54.0	8.51	11218	14282	−3065	$Sr^+ + Sr + Yb$
Ba_2Mg^+	61.3	7.83	11995	11944	51	$Ba^+ + Ba + Mg$
Ba_2Ca^+	59.6	8.10	14015	14857	−842	$Ba^+ + Ba + Ca$
Ba_2Sr^+	57.8	8.42	13891	15860	−1969	$Ba^+ + Ba + Sr$
Ba_3^+	57.5	8.52	15382	17643	−2261	$Ba^+ + Ba + Ba$
Ba_2Yb^+	58.7	8.45	12008	13163	−1155	$Ba^+ + Ba + Yb$

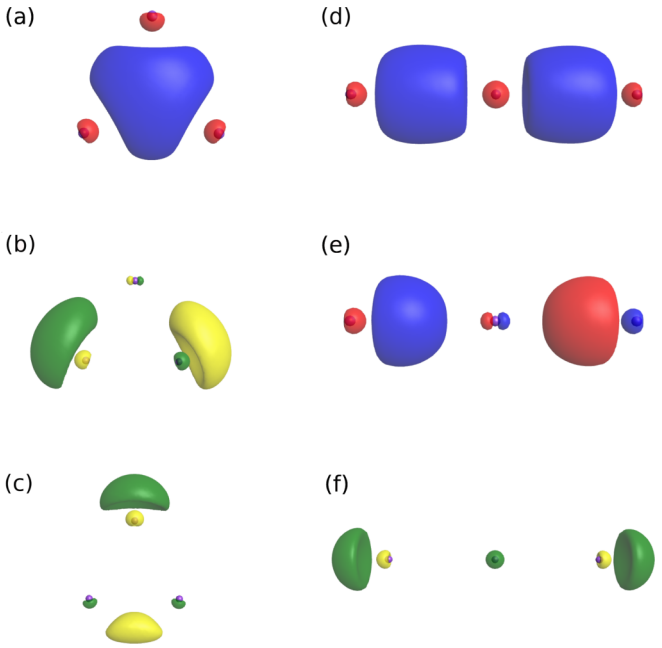

FIG. 4. Molecular orbital isosurfaces of homonuclear alkali-metal triatomic molecular ions in the singlet $^1A_1$ electronic state having the $^1A'_1$ symmetry within the D_{3h} point group at the equilibrium triangular geometry—(a) closed-shell a'_1 HOMO, (b) e' LUMO, and (c) e' LUMO + 1—and in the triplet $^3B_2$ electronic state having the $^3\Sigma_u^+$ symmetry within the $C_{\infty v}$ point group at the equilibrium linear geometry: (d) open-shell σ_g HOMO-1, (e) open-shell σ_u HOMO, and (f) σ_g LUMO.

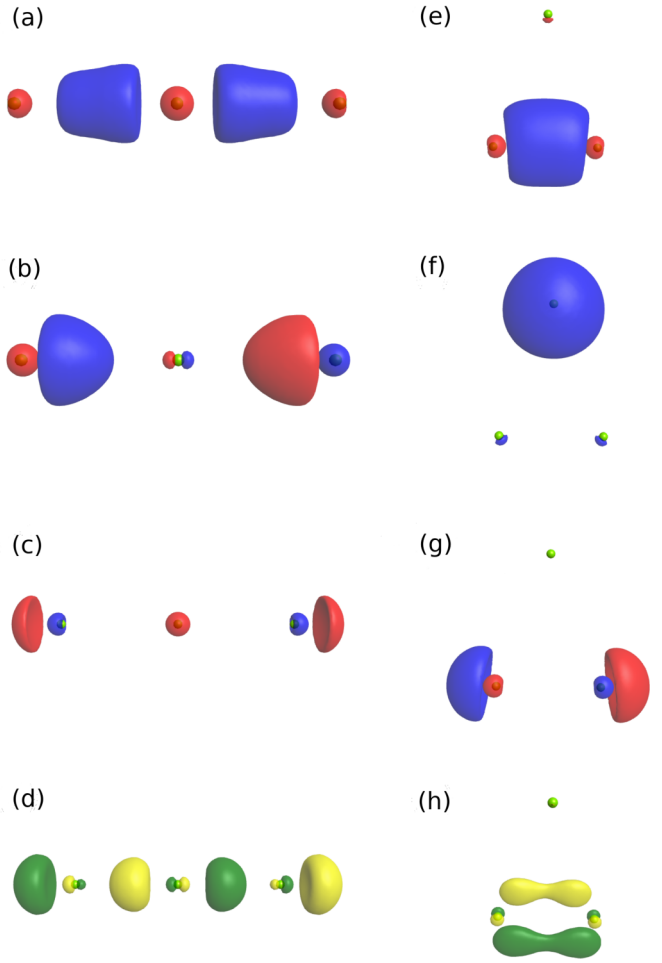

FIG. 5. Molecular orbital isosurfaces of homonuclear alkaline-earth-metal triatomic molecular ions in the doublet $^2A_1$ electronic state having the $^2\Sigma^+_g$ symmetry within the $C_{\infty v}$ point group at the equilibrium linear geometry—(a) closed-shell σ_g HOMO-2, (b) closed-shell σ_u HOMO-1, (c) open-shell σ_g HOMO, and (d) σ_u LUMO—and in the doublet $^2B_2$ electronic state within the C_{2v} point group at the equilibrium triangular geometry: (e) closed-shell a_1 HOMO-2, (f) closed-shell a_1 HOMO-1, (g) open-shell b_2 HOMO, and (h) b_1 LUMO.

To explain the different triangular and linear equilibrium geometries of the lowest singlet and triplet electronic states of the alkali-metal triatomic molecular ions, in Fig. 4, we plot exemplary isosurfaces of highest occupied molecular orbitals (HOMOs) and lowest unoccupied molecular orbitals (LUMOs) for a homonuclear case of these ions. Molecular orbitals for heteronuclear ions look very similar with small alterations due to the broken symmetry. In the singlet state, two valence electrons occupy a single orbital which is highly bonding due to a significant charge delocalization and large electron density between nuclei [see Fig. 4(a)]. Two plotted LUMOs are antibonding and degenerate for homonuclear ions. In the triplet state, however, one electron has to be excited from the lowest valence orbital. The second valence orbital has antibonding character at triangular geometry [see Fig. 4(b)], whereas it starts to be bonding at the linear geometry [see Fig. 4(e)]. Thus, at the linear geometry, two occupied orbitals in the triplet state have bonding character with large electron densities between nuclei that stabilize the triplet-state molecular ions.

Alkaline-earth-metal triatomic molecular ions A_2B^+ have five valence electrons occupying two closed-shell and one open-shell valence orbitals in the lowest doublet electronic states (see Fig. 5), therefore these ions have a richer structure of possible equilibrium geometries as compared with alkali-metal ions. Their electronic ground state can have either doublet $^2A_1$ or $^2B_2$ symmetry within the C_{2v} point group. Interestingly, for both electronic symmetries there may exist two minima, the first one at an isosceles triangular geometry with the B atom on the symmetry axis within the C_{2v} point group, and the second one at a linear or close to linear geometry.

Among homonuclear triatomic alkaline-earth-metal molecular ions, A_3^+, Mg_3^+, Ca_3^+, and Sr_3^+ have their ground state of the $^2A_1$ symmetry, while Ba_3^+ has the $^2B_2$ symmetry ground state. In the $^2A_1$ state, Mg_3^+ has a single global minimum of the $^2\Sigma_g^+$ symmetry at the linear geometry, while Ca_3^+, Sr_3^+, and Ba_3^+ have two local minima. For Ca_3^+, the minimum at the linear geometry is the global minimum. For Sr_3^+ and Ba_3^+ there are two local minima at triangular geometries, one with acute and one with obtuse (close to 180°) angles. In the $^2A_1$ state, the global minimum of Sr_3^+ is at an obtuse angle while the global minimum of Ba_3^+ is at an acute angle. PESs for Ca_3^+ and Ba_3^+ in the $^2A_1$ and $^2B_2$ electronic states are presented in Fig. 6. For both ions and both states, two local minima are clearly visible. In the $^2A_1$ state, two minima have similar well depths, while in the $^2B_2$

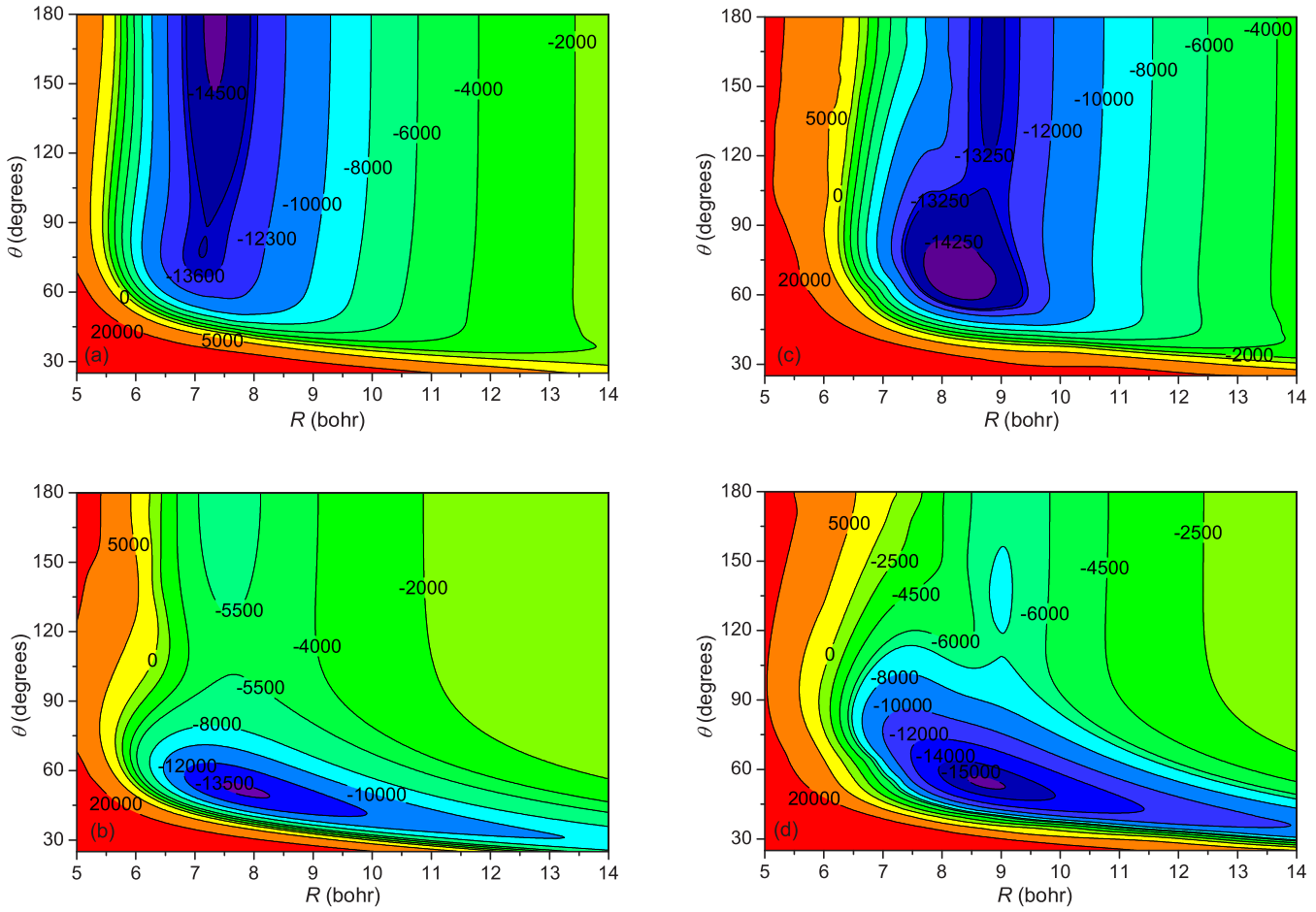

FIG. 6. Two-dimensional cuts through the ground-state potential-energy surfaces of homonuclear alkaline-earth-metal triatomic molecular ions: (a) Ca_3^+ in the $^2A_1$ electronic state, (b) Ca_3^+ in the $^2B_2$ electronic state, (c) Ba_3^+ in the $^2A_1$ electronic state, and (d) Ba_3^+ in the $^2B_2$ electronic state.

state the minima at the acute triangular geometry have much larger well depths. Therefore in Table IX we report global minima of the $^2B_2$ state only.

Heteronuclear alkaline-earth-metal molecular ions A_2B^+ have an additional local minimum at the asymmetric AAB^+ linear geometry of the $^2A_1$ state which coreduces to the $^2\Sigma^+$ symmetry and has a similar well depth as other minima. The Sr_2Mg^+, Sr_2Yb^+, Ba_2Mg^+, Ba_2Ca^+, Ba_2Sr^+, and Ba_2Yb^+ molecular ions have their ground state of the $^2B_2$ symmetry at the acute triangular geometry. All remaining heteronuclear alkaline-earth-metal trimers, notably all of the compounds with two Mg or Ca atoms, have their ground state of the $^2A_1$ symmetry with a variety of geometries from symmetric linear to acute or obtuse triangular ones and asymmetric linear ones. Interestingly, all heteronuclear molecular ions containing one Yb atom have their ground state at the asymmetric linear geometry. Among all alkaline-earth-metal triatomic molecular ions, the Mg_3^+ ion in the $^2A_1$ state is the most strongly bound with $D_e = 16\,408\,\mathrm{cm}^{-1}$, followed by other homonuclear ions in the $^2A_1$ and $^2B_2$ states. On the other hand, heteronuclear alkaline-earth-metal molecular ions containing two Mg atoms are the most weakly bound. The Mg_2Ba^+ ion at the symmetric close-to-linear geometry in the $^2A_1$ state has the well depth of $D_e = 6386\,\mathrm{cm}^{-1}$, the same $MgMgBa^+$ ion at the asymmetric linear geometry in the $^2A_1$ state has a well depth of $D_e = 3744\,\mathrm{cm}^{-1}$, and Mg_2Ba^+ does not have a minimum in the $^2B_2$ state.

Equilibrium internuclear distances in alkaline-earth-metal triatomic molecular ions are smaller or larger than equilibrium distances of the corresponding ionic and neutral dimers, depending on the triatomic ions' electronic state and geometry. For the linear geometry, both symmetric and asymmetric molecular ions generally have larger equilibrium distances. For the isosceles triangular geometry, the molecular ions in the $^2A_1$ electronic state have the distance between A and B atoms (the legs of the triangle) smaller while between two A atoms (the base of the triangle) larger as compared with the corresponding ionic dimers, while the molecular ions in the $^2B_2$ electronic state show the opposite pattern.

To understand the different equilibrium geometries of the alkaline-earth-metal triatomic molecular ions, in Fig. 5, we plot exemplary isosurfaces of valence orbitals for a homonuclear case of these ions in the $^2A_1$ electronic state at the linear geometry and in the $^2B_2$ electronic state at the triangular geometry. Molecular orbitals for heteronuclear ions look similar with small alterations due to the broken symmetry.

Interestingly, the molecular orbitals of the $^2A_1$ electronic state having the $^2\Sigma_g^+$ symmetry at the linear geometry resemble the molecular orbitals of the alkali-metal triatomic molecular ions in the triplet $^3B_2$ electronic state having the $^3\Sigma_u^+$ symmetry at the same geometry. Two lowest closed-shell valence orbitals have bonding character with large electron densities between nuclei that stabilize the linear molecular ions [see Figs. 5(a) and 5(b)]. The bonding character of the second valence orbital is reduced for triangular geometries, thus the linear minimum of the $^2A_1$ electronic state is relatively stabilized. On the other hand, the electron delocalization is reduced in molecular valence orbitals for alkaline-earth-metal triatomic molecular ions in the $^2B_2$ electronic state. In fact, the structure of molecular orbitals for this state can be well described as a sum of molecular orbitals of an A_2^+ diatomic molecular ion in the $^2\Sigma_u$ electronic state and a ground-state B atom. Thus no proper chemical bonding is present in the $^2B_2$ electronic state and the acute triangular geometry is favored for this state because of steric effects. The interplay of the structure of molecular orbitals and the correlation of valence electrons results in two local minima for most of the symmetric alkaline-earth-metal triatomic molecular ions in contrast to alkali-metal ions.

Interestingly, homonuclear alkaline-earth-metal triatomic molecular ions have a permanent electric dipole moments along their symmetry axis. In the $^2B_2$ electronic state, Mg_3^+, Ca_3^+, Sr_3^+, and Ba_3^+ have permanent electric dipole moments of 1.71, 0.33, 0.51, and 0.77 D, respectively. Obtained permanent electric dipole moments are in agreement with the picture presented using molecular orbital description of $^2B_2$-state molecular ions as $A_2^+ + B$ in the previous paragraph. Additionally, calculations of partial electric charges, e.g., using Hirshfeld analysis, confirm the favored charge localization at A_2^+. Heteronuclear alkaline-earth-metal triatomic molecular ions have larger permanent electric dipole moments of the order of magnitude as in diatomic molecular ions.

Three-body interaction destabilizes all alkaline-earth-metal triatomic molecular ions in the $^2A_1$ electronic state at the acute triangular geometry and almost all ions in the $^2B_2$ electronic state with the exception of Ba_2Mg^+. The largest destabilizing three-body energy terms are for homonuclear ions with the largest value of $D_{3b} = -5452\,\mathrm{cm}^{-1}$ for Ca_3^+ in the $^2A_1$ state at the triangular geometry. Interestingly, for the $^2A_1$ electronic state at the linear geometry, the effect of three-body interactions is analogous as for alkali-metal molecular ions in the $^3B_2$ at the same geometry. That is, the three-body interaction stabilizes all the asymmetric AAB^+ ions while the symmetric ABA^+ ones are stabilized only if the ionization potential of A is larger than that of B.

Unfortunately, for alkaline-earth-metal triatomic molecular ions, the ambiguity in the decomposition of the interaction energy into two-body or three-body contributions is larger than for alkali-metal ions. In fact, the sign of three-body energies can change for some ions, if another assignment of the charge to the monomers is employed. The most striking examples are homonuclear triangular ions in the $^2A_1$ electronic state which do not form equilateral triangles and for which the three-body energy changes by a few thousand cm^{-1} for different charge assignments. Detailed studies of unambiguous many-body energy decomposition in ionic systems are out of the scope of the present paper.

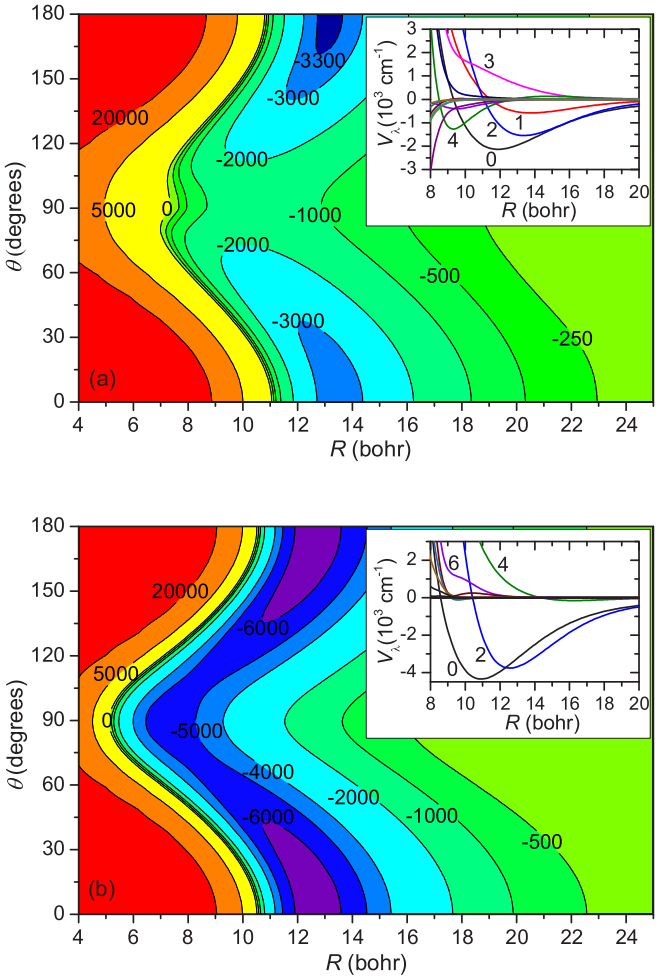

FIG. 7. Two-dimensional cuts through the ground-state potential-energy surfaces of (a) $KRb^+ + K$ and (b) $Rb^+ + Sr_2$ ion-neutral systems. Insets show the corresponding Legendre components.

C. Chemical reactions in ion-neutral systems

The prospects for sympathetic cooling and applications of molecular ions immersed into ultracold atomic gases or atomic ions immersed into ultracold molecular gases can be jeopardized by possible chemical reactions, on one hand. However, cold and controlled chemical reactions in these systems can be an interesting subject of study on its own, on the other hand [39–46].

To study chemical reactions, potential-energy surfaces of adequate quality are needed. In Fig. 7, we present exemplary nonreactive two-dimensional PESs within the rigid rotor approximation for high-spin interaction between the KRb^+ molecular ion and K atom, and between the Rb^+ atomic ion and Sr_2 molecule. PESs are shown together with their decompositions onto Legendre components. Both surfaces are very anisotropic, with the first and second anisotropic Legendre component almost as large as the isotropic one. This suggests large inelastic rate coefficients for collisional rotational relaxation in the considered systems. PESs for other nonreactive systems using the presented methodology can be computed upon request. We will study the potential-energy

surfaces for reactive ion-neutral collisions in triatomic alkali-metal and alkaline-earth-metal systems in the future, while in the next paragraphs we analyze possible channels of chemical reactions based on the energetics of the reactants.

In the considered diatomic ion-atom systems there can be several paths of collision- and interaction-induced chemical reactions related to the charge rearrangement [8]. The radiative charge transfer

$$A^+ + B \to A + B^+ + \hbar\omega, \tag{3}$$

where the electron is spontaneously transferred from the B atom to the A^+ ion emitting a photon of energy $\hbar\omega$. This process is possible when the ionization potential of the neutral A atom is not smaller than the ionization potential of the B atom [149]:

$$\mathrm{IP}(A) \geqslant \mathrm{IP}(B). \tag{4}$$

The nonradiative charge transfer driven by nonadiabatic couplings can also be possible for the same energetic condition if electronic states associated with $A^+ + B$ and $A + B^+$ thresholds form an avoided crossing at shorter internuclear distances. The radiative association

$$A^+ + B \to AB^+(v, j) + \hbar\omega, \tag{5}$$

where the A^+ ion and the B atom spontaneously form a AB^+ molecular ion in a (v, j) rovibrational state emitting a photon of energy $\hbar\omega$. Such a process driven by the transition between two electronic states is possible when the reaction (3) is energetically allowed or when the interaction energy in the AB^+ molecular ion is larger than or equal to the missing difference of the ionization potentials. The spontaneous radiative association is also possible (but very unlikely) for all polar complexes AB^+ driven by the transition between rovibrational levels of the electronic ground state. Finally, the spontaneous radiative deexcitation of the formed AB^+ molecular ion in an excited (v, j) rovibrational level to lower-energy levels is feasible:

$$AB^+(v, j) \to AB^+(v', j \pm 1) + \hbar\omega. \tag{6}$$

Energetics of reactions given by Eqs. (3) and (5) can be assigned by using the data from Table I.

In the considered triatomic ion-atom systems, combinations of ultracold molecular ions with atoms, $AB^+ + C$, or atomic ions with molecules, $A^+ + BC$, lead to a broad range of possible chemical reactions related to the charge or atom rearrangement. Their possibility and energetics can be assigned by using the atomic and molecular data provided in the present paper and collected in Tables I–IX together with previous results for neutral molecules [56,91].

The nonradiative (or radiative) charge transfer

$$\begin{aligned} AB^+ + C &\to AB + C^+ \ (+\hbar\omega), \\ A^+ + BC &\to A + BC^+ \ (+\hbar\omega) \end{aligned} \tag{7}$$

is possible when the electron attachment energy of the AB^+ molecular ion or A^+ ion is not smaller than the ionization potential of the neutral C atom or BC molecule:

$$\begin{aligned} \mathrm{EA}(AB^+) &\geqslant \mathrm{IP}(C), \\ \mathrm{EA}(A^+) &\geqslant \mathrm{IP}(BC), \end{aligned} \tag{8}$$

where $\mathrm{EA}(A^+) = \mathrm{IP}(A)$, while $\mathrm{EA}(AB^+) \approx \mathrm{IP}(AB)$ for systems with diagonal Franck-Condon factors between levels of AB^+ and AB. The radiative association is also possible for the same energetic conditions:

$$\begin{aligned} AB^+ + C &\to ABC^+ + \hbar\omega, \\ A^+ + BC &\to ABC^+ + \hbar\omega. \end{aligned} \tag{9}$$

The nonradiative (or radiative) ion-exchange reaction

$$AB^+ + C \to A + BC^+ \ (+\hbar\omega) \tag{10}$$

is possible when the dissociation energy of AB^+ is not larger than the dissociation energy of BC^+, provided lack of charge transfer between B^+ and C:

$$D_0(BC^+) \geqslant D_0(AB^+) \quad \text{for} \quad \mathrm{IP}(B) \leqslant \mathrm{IP}(C). \tag{11}$$

If the charge transfer between B^+ and C is possible, the above condition has to be corrected:

$$D_0(BC^+) + \mathrm{IP}(B) - \mathrm{IP}(C) \geqslant D_0(AB^+) \quad \text{for} \quad \mathrm{IP}(B) > \mathrm{IP}(C). \tag{12}$$

The radiative or nonradiative atom-exchange reaction

$$AB^+ + C \to A^+ + BC \ (+\hbar\omega) \tag{13}$$

is possible when the dissociation energy of AB^+ is not larger than the dissociation energy of BC, provided the ionization potential of A is not larger than the ionization potential of B:

$$D_0(BC) \geqslant D_0(AB^+) \quad \text{for} \quad \mathrm{IP}(A) \leqslant \mathrm{IP}(B). \tag{14}$$

If the ionization potential of A is larger than that of B, the above condition has to be corrected:

$$D_0(BC^+) \geqslant D_0(AB^+) + \mathrm{IP}(A) - \mathrm{IP}(B) \quad \text{for} \quad \mathrm{IP}(A) > \mathrm{IP}(B). \tag{15}$$

The reverse reaction to the one given by Eq. (13) is possible for reversed conditions of Eqs. (14) and (15).

The collisional dissociation associated with the charge transfer

$$\begin{aligned} AB^+ + C &\to A + B + C^+, \\ A^+ + BC &\to A + B + C^+ \end{aligned} \tag{16}$$

is possible when the ionization potential of A is larger than the ionization potential of C by more than the dissociation energy of AB^+ or BC:

$$\begin{aligned} \mathrm{IP}(A) - \mathrm{IP}(C) &\geqslant D_0(AB^+), \\ \mathrm{IP}(A) - \mathrm{IP}(C) &\geqslant D_0(BC). \end{aligned} \tag{17}$$

In the case of rovibrationally exited molecular ions, the collision-induced deexcitation may also happen:

$$AB^+(v, j) + C \to AB^+(v', j') + C. \tag{18}$$

In the case of linear molecular ions, the collision-induced isomerization is possible:

$$ABA^+(\{v\}, j) + C \leftrightarrow AAB^+(\{v'\}, j') + C, \tag{19}$$

where the reaction direction depends on which isomer has a larger energy. The minimum-energy reaction paths for the spontaneous isomerization of selected alkali-metal triatomic

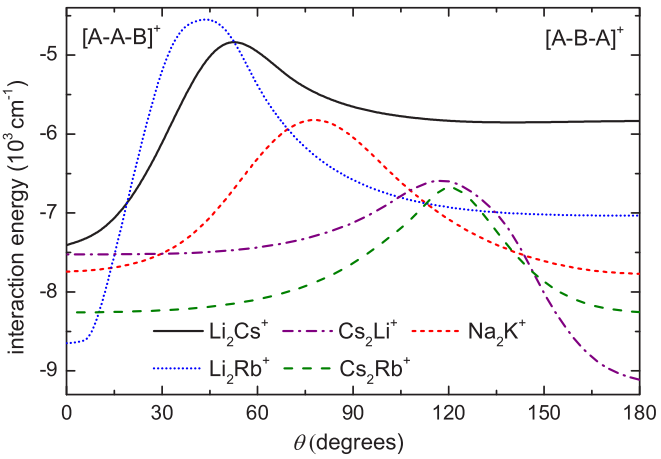

FIG. 8. Minimum-energy reaction paths for the isomerization of selected alkali-metal triatomic molecular ions between their asymmetric AAB^+ and symmetric ABA^+ forms.

molecular ions are presented in Fig. 8. The spontaneous isomerization is strongly suppressed because of the large energy barriers, nevertheless the heights of those barriers give a good estimation of the interaction energy needed to allow for collision-induced isomerization.

The intermolecular charge-transfer reactions

$$AB + CD^+ \rightarrow AB^+ + CD \tag{20}$$

are possible when the ionization potential of AB is not smaller than the ionization potential of CD. The energetics of the atom- and ion-exchange reactions

$$\begin{aligned} AB + CD^+ &\rightarrow AC + BD^+, \\ AB + CD^+ &\rightarrow AC^+ + BD \end{aligned} \tag{21}$$

can also be assigned using the dissociation and ionization energies of involved molecules and molecular ions.

If molecular reactants are not in the ground vibrational level ($v = 0$), then their dissociation energies D_0 in all the above conditions should be replaced by dissociation energies for the considered vibrational level, D_v. If the reaction energy is smaller than the uncertainty of the calculated dissociation and ionization energies, then the above-predicted energetics may be less accurate.

If the above-considered reactions are energetically forbidden, they may potentially be induced by the laser-field excitation of involved reactants [11,44,45]. If the excitation energy to the lowest excited electronic state of one of the atomic or molecular reactants is larger than the missing reaction energy then the endoenergetic chemical reaction on the ground potential-energy surface becomes exoenergetic on the electronically excited potential-energy surface [41].

Finally, the presented atomic and molecular data also allow one to assign energetics of ionic chemical reactions

$$\begin{aligned} AB^+ + AB^+ &\rightarrow A_2^+ + B_2^+, \\ AB^+ + CD^+ &\rightarrow AC^+ + BD^+, \\ AB^+ + C^+ &\rightarrow A^+ + BC^+, \end{aligned} \tag{22}$$

however such reactions are not relevant for ultracold systems due to the highly repulsive nature of the Coulomb interaction.

IV. SUMMARY AND CONCLUSIONS

Experiments employing ultracold molecular ions and ion-neutral mixtures are a promising platform to further our understanding of the physical basis of chemistry and to perform high-precision measurements essential for testing fundamental laws of nature. Compared to neutral molecules, molecular ions are easier to prepare, trap, and detect. In this paper, we have presented theoretical results for all ground-state diatomic AB^+ and most of the triatomic A_2B^+ molecular ions consisting of alkali-metal and alkaline-earth-metal atoms. We have employed *ab initio* techniques of quantum chemistry, such as the coupled cluster method restricted to single, double, and noniterative triple excitations, CCSD(T), combined with large Gaussian basis sets and small-core energy-consistent pseudopotentials, to obtain equilibrium distances, atomization energies, ionization potentials, permanent electric dipole moments, and polarizabilities.

We have predicted a wide range of dissociation energies and permanent electric dipole moments for the dimers, and a variety of equilibrium geometries for the trimers from equilateral triangular through isosceles triangular to linear. We have also evaluated and characterized three-body nonadditive interactions in these systems at equilibrium geometries. We have identified possible channels of chemical reactions in ionic two-body $A^+ + B$ and AB^+ and three-body $A^+ + AB$, $AB^+ + A$, and A_2B^+ systems, based on the energetics of the reactants. Additionally, we have provided two-dimensional interaction potential-energy surfaces for $KRb^+ + K$ and $Sr_2 + Rb^+$ mixtures and we have presented example calculations of minimum-energy paths for the isomerization reaction of linear alkaline-metal trimers in the lowest triplet electronic state between asymmetric AAB^+ and symmetric ABA^+ arrangements. PESs for other systems can be computed upon request.

The present results may be useful for investigating controlled chemical reactions and other applications of alkali-metal and alkaline-earth molecular ions immersed in or formed from ultracold gases. Collected molecular properties can be employed in quantum scattering calculations or easily used to access chemical characteristics of selected systems realized in modern cold hybrid ion-neutral experiments. In the future, we plan to use the calculated potential-energy surfaces to study two-body and three-body collisions in ion-neutral systems and to extend the presented results for three-body interactions of atomic and molecular ions with atoms or molecules in excited electronic states.

ACKNOWLEDGMENTS

We would like to thank Tatiana Korona for many useful discussions and help with the MOLPRO and Gaussian programs. We acknowledge support from the National Science Centre Poland (Grants No. 2016/23/B/ST4/03231 and No. 2015/19/D/ST4/02173) and the PL-Grid Infrastructure.

[1] D. DeMille, J. M. Doyle, and A. O. Sushkov, Science **357**, 990 (2017).
[2] C. Gross and I. Bloch, Science **357**, 995 (2017).
[3] J. L. Bohn, A. M. Rey, and J. Ye, Science **357**, 1002 (2017).
[4] D. J. Wineland, Rev. Mod. Phys. **85**, 1103 (2013).
[5] S. Haroche, Rev. Mod. Phys. **85**, 1083 (2013).
[6] A. Härter and J. H. Denschlag, Contemp. Phys. **55**, 33 (2014).
[7] R. Côté, Adv. At. Mol. Opt. Phys. **65**, 67 (2016).
[8] M. Tomza, K. Jachymski, R. Gerritsma, A. Negretti, T. Calarco, Z. Idziaszek, and P. S. Julienne, Rev. Mod. Phys. **91**, 035001 (2019).
[9] A. T. Grier, M. Cetina, F. Oručević, and V. Vuletić, Phys. Rev. Lett. **102**, 223201 (2009).
[10] F. H. Hall, P. Eberle, G. Hegi, M. Raoult, M. Aymar, O. Dulieu, and S. Willitsch, Mol. Phys. **111**, 2020 (2013).
[11] S. T. Sullivan, W. G. Rellergert, S. Kotochigova, and E. R. Hudson, Phys. Rev. Lett. **109**, 223002 (2012).
[12] W. G. Rellergert, S. T. Sullivan, S. Kotochigova, A. Petrov, K. Chen, S. J. Schowalter, and E. R. Hudson, Phys. Rev. Lett. **107**, 243201 (2011).
[13] C. Zipkes, S. Palzer, C. Sias, and M. Köhl, Nature (London) **464**, 388 (2010).
[14] S. Haze, S. Hata, M. Fujinaga, and T. Mukaiyama, Phys. Rev. A **87**, 052715 (2013).
[15] F. H. J. Hall, M. Aymar, N. Bouloufa-Maafa, O. Dulieu, and S. Willitsch, Phys. Rev. Lett. **107**, 243202 (2011).
[16] W. Smith, D. Goodman, I. Sivarajah, J. Wells, S. Banerjee, R. Côté, H. Michels, J. A. Mongtomery, and F. Narducci, Appl. Phys. B **114**, 75 (2014).
[17] J. Joger, H. Fürst, N. Ewald, T. Feldker, M. Tomza, and R. Gerritsma, Phys. Rev. A **96**, 030703(R) (2017).
[18] H. Fürst, T. Feldker, N. V. Ewald, J. Joger, M. Tomza, and R. Gerritsma, Phys. Rev. A **98**, 012713 (2018).
[19] Z. Meir, T. Sikorsky, R. Ben-shlomi, N. Akerman, Y. Dallal, and R. Ozeri, Phys. Rev. Lett. **117**, 243401 (2016).
[20] K. Ravi, S. Lee, A. Sharma, G. Werth, and S. Rangwala, Nat. Commun. **3**, 1126 (2012).
[21] A. Härter, A. Krükow, A. Brunner, W. Schnitzler, S. Schmid, and J. H. Denschlag, Phys. Rev. Lett. **109**, 123201 (2012).
[22] I. Sivarajah, D. S. Goodman, J. E. Wells, F. A. Narducci, and W. W. Smith, Phys. Rev. A **86**, 063419 (2012).
[23] R. Côté and A. Dalgarno, Phys. Rev. A **62**, 012709 (2000).
[24] F. H. J. Hall and S. Willitsch, Phys. Rev. Lett. **109**, 233202 (2012).
[25] T. Sikorsky, Z. Meir, R. Ben-shlomi, N. Akerman, and R. Ozeri, Nat. Comm. **9**, 920 (2018).
[26] L. Ratschbacher, C. Zipkes, C. Sias, and M. Kohl, Nat. Phys. **8**, 649 (2012).
[27] U. Bissbort, D. Cocks, A. Negretti, Z. Idziaszek, T. Calarco, F. Schmidt-Kaler, W. Hofstetter, and R. Gerritsma, Phys. Rev. Lett. **111**, 080501 (2013).
[28] H. Doerk, Z. Idziaszek, and T. Calarco, Phys. Rev. A **81**, 012708 (2010).
[29] M. Tomza, C. P. Koch, and R. Moszynski, Phys. Rev. A **91**, 042706 (2015).
[30] H. da Silva Jr, M. Raoult, M. Aymar, and O. Dulieu, New J. Phys. **17**, 045015 (2015).
[31] F. H. Hall, M. Aymar, M. Raoult, O. Dulieu, and S. Willitsch, Mol. Phys. **111**, 1683 (2013).
[32] A. Krükow, A. Mohammadi, A. Härter, J. H. Denschlag, J. Pérez-Ríos, and C. H. Greene, Phys. Rev. Lett. **116**, 193201 (2016).
[33] J. Wolf, M. Deiß, A. Krükow, E. Tiemann, B. P. Ruzic, Y. Wang, J. P. D'Incao, P. S. Julienne, and J. H. Denschlag, Science **358**, 921 (2017).
[34] S. T. Sullivan, W. G. Rellergert, S. Kotochigova, K. Chen, S. J. Schowalter, and E. R. Hudson, Phys. Chem. Chem. Phys. **13**, 18859 (2011).
[35] S. Jyothi, T. Ray, S. Dutta, A. R. Allouche, R. Vexiau, O. Dulieu, and S. A. Rangwala, Phys. Rev. Lett. **117**, 213002 (2016).
[36] T. Schmid, C. Veit, N. Zuber, R. Löw, T. Pfau, M. Tarana, and M. Tomza, Phys. Rev. Lett. **120**, 153401 (2018).
[37] W. G. Rellergert, S. T. Sullivan, S. J. Schowalter, S. Kotochigova, K. Chen, and E. R. Hudson, Nature (London) **495**, 490 (2013).
[38] A. K. Hansen, O. Versolato, S. Kristensen, A. Gingell, M. Schwarz, A. Windberger, J. Ullrich, J. C. López-Urrutia, M. Drewsen *et al.*, Nature (London) **508**, 76 (2014).
[39] J. Deiglmayr, A. Göritz, T. Best, M. Weidemüller, and R. Wester, Phys. Rev. A **86**, 043438 (2012).
[40] M. Tomza, Phys. Rev. Lett. **115**, 063201 (2015).
[41] P. Puri, M. Mills, C. Schneider, I. Simbotin, J. A. Montgomery, R. Côté, A. G. Suits, and E. R. Hudson, Science **357**, 1370 (2017).
[42] A. Kilaj, H. Gao, D. Rösch, U. Rivero, J. Küpper, and S. Willitsch, Nat. Comm. **9**, 2096 (2018).
[43] M. Tomza, Phys. Chem. Chem. Phys. **19**, 16512 (2017).
[44] A. D. Dörfler, P. Eberle, D. Koner, M. Tomza, M. Meuwly, and S. Willitsch, Nat. Commun. **10**, 5429 (2019).
[45] P. Puri, M. Mills, I. Simbotin, J. A. Montgomery, R. Côté, C. Schneider, A. G. Suits, and E. R. Hudson, Nat. Chem. **11**, 615 (2019).
[46] M. Kas, J. Loreau, J. Liévin, and N. Vaeck, Phys. Rev. A **99**, 042702 (2019).
[47] M. Germann, X. Tong, and S. Willitsch, Nat. Phys. **10**, 820 (2014).
[48] W. B. Cairncross, D. N. Gresh, M. Grau, K. C. Cossel, T. S. Roussy, Y. Ni, Y. Zhou, J. Ye, and E. A. Cornell, Phys. Rev. Lett. **119**, 153001 (2017).
[49] B. Midya, M. Tomza, R. Schmidt, and M. Lemeshko, Phys. Rev. A **94**, 041601(R) (2016).
[50] B. v. Issendorff and O. Cheshnovsky, Annu. Rev. Phys. Chem. **56**, 549 (2005).
[51] P. Soldán, M. T. Cvitaš, and J. M. Hutson, Phys. Rev. A **67**, 054702 (2003).
[52] P. Soldán, Phys. Rev. A **77**, 054501 (2008).
[53] J. Klos, P. S. Zuchowski, L. Rajchel, G. Chalasinski, and M. M. Szczesniak, J. Chem. Phys. **129**, 134302 (2008).
[54] P. Soldán, Phys. Rev. A **82**, 034701 (2010).
[55] P. Soldan, J. Chem. Phys. **132**, 234308 (2010).
[56] M. Tomza, K. W. Madison, R. Moszynski, and R. V. Krems, Phys. Rev. A **88**, 050701(R) (2013).
[57] I. G. Kaplan, J. Hernández-Cobos, I. Ortega-Blake, and O. Novaro, Phys. Rev. A **53**, 2493 (1996).
[58] I. G. Kaplan, S. Roszak, and J. Leszczynski, J. Chem. Phys. **113**, 6245 (2000).
[59] G. Bravo-Pérez, I. Garzón, and O. Novaro, Chem. Phys. Lett. **313**, 655 (1999).

[60] D. Danovich and S. Shaik, J. Chem. Theory Comput. **6**, 1479 (2010).

[61] A. W. Castleman and R. G. Keesee, Chem. Rev. **86**, 589 (1986).

[62] E. J. Bieske and O. Dopfer, Chem. Rev. **100**, 3963 (2000).

[63] D. Pavolini and F. Spiegelmann, J. Chem. Phys. **87**, 2854 (1987).

[64] F. Spiegelmann and D. Pavolini, J. Chem. Phys. **89**, 4954 (1988).

[65] S. N. Khanna, F. Reuse, and J. Buttet, Phys. Rev. Lett. **61**, 535 (1988).

[66] G.-H. Jeung, M. Broyer, and P. Labastie, Chem. Phys. Lett. **165**, 494 (1990).

[67] W. A. de Heer, Rev. Mod. Phys. **65**, 611 (1993).

[68] A. Martínez and A. Vela, Phys. Rev. B **49**, 17464 (1994).

[69] B. Smart, C. Marsden, J. M. Hughes, F. Wang, and E. I. von Nagy-Felsobuki, J. Mol. Struct. **376**, 449 (1996).

[70] A. Lyalin, I. A. Solov'yov, A. V. Solov'yov, and W. Greiner, Phys. Rev. A **75**, 053201 (2007).

[71] G. D. Purvis III and R. J. Bartlett, J. Chem. Phys. **76**, 1910 (1982).

[72] P. J. Knowles, C. Hampel, and H.-J. Werner, J. Chem. Phys. **99**, 5219 (1993).

[73] S. Boys and F. Bernardi, Mol. Phys. **19**, 553 (1970).

[74] B. P. Prascher, D. E. Woon, K. A. Peterson, T. H. Dunning, and A. K. Wilson, Theor. Chem. Acc. **128**, 69 (2010).

[75] M. Dolg and X. Cao, Chem. Rev. **112**, 403 (2012).

[76] I. S. Lim, H. Stoll, and P. Schwerdtfeger, J. Chem. Phys. **124**, 034107 (2006).

[77] Y. Wang and M. Dolg, Theor. Chem. Acc. **100**, 124 (1998).

[78] M. Tomza, F. Pawlowski, M. Jeziorska, C. P. Koch, and R. Moszynski, Phys. Chem. Chem. Phys. **13**, 18893 (2011).

[79] M. Tomza, W. Skomorowski, M. Musial, R. Gonzalez Ferez, C. P. Koch, and R. Moszynski, Mol. Phys. **111**, 1781 (2013).

[80] M. Tomza, Phys. Rev. A **88**, 012519 (2013).

[81] M. Tomza, Phys. Rev. A **90**, 022514 (2014).

[82] F.-M. Tao and Y.-K. Pan, J. Chem. Phys. **97**, 4989 (1992).

[83] A. Miffre, M. Jacquey, M. Büchner, G. Trénec, and J. Vigué, Eur. Phys. J. D **38**, 353 (2006).

[84] Z.-C. Yan, J. F. Babb, A. Dalgarno, and G. W. F. Drake, Phys. Rev. A **54**, 2824 (1996).

[85] NIST Atomic Spectra Database, http://physics.nist.gov/PhysRefData/ASD.

[86] C. R. Ekstrom, J. Schmiedmayer, M. S. Chapman, T. D. Hammond, and D. E. Pritchard, Phys. Rev. A **51**, 3883 (1995).

[87] J. Kaur, D. K. Nandy, B. Arora, and B. K. Sahoo, Phys. Rev. A **91**, 012705 (2015).

[88] M. D. Gregoire, I. Hromada, W. F. Holmgren, R. Trubko, and A. D. Cronin, Phys. Rev. A **92**, 052513 (2015).

[89] S. G. Porsev and A. Derevianko, J. Chem. Phys. **119**, 844 (2003).

[90] S. G. Porsev and A. Derevianko, J. Exp. Theor. Phys. **102**, 195 (2006).

[91] P. S. Żuchowski and J. M. Hutson, Phys. Rev. A **81**, 060703(R) (2010).

[92] S. G. Porsev, M. S. Safronova, A. Derevianko, and C. W. Clark, Phys. Rev. A **89**, 012711 (2014).

[93] H.-J. Werner, P. J. Knowles, G. Knizia, F. R. Manby, M. Schütz, P. Celani, T. Korona, R. Lindh, A. Mitrushenkov, G. Rauhut, K. R. Shamasundar, T. B. Adler, R. D. Amos, A. Bernhardsson, A. Berning, D. L. Cooper, M. J. O. Deegan, A. J. Dobbyn, F. Eckert, E. Goll, C. Hampel, A. Hesselmann, G. Hetzer, T. Hrenar, G. Jansen, C. Köppl, Y. Liu, A. W. Lloyd, R. A. Mata, A. J. May, S. J. McNicholas, W. Meyer, M. E. Mura, A. Nicklass, D. P. O'Neill, P. Palmieri, D. Peng, K. Pflüger, R. Pitzer, M. Reiher, T. Shiozaki, H. Stoll, A. J. Stone, R. Tarroni, T. Thorsteinsson, and M. Wang, MOLPRO, version 2012.1, a package of *ab initio* programs, 2012, http://www.molpro.net.

[94] M. J. Frisch, G. W. Trucks, H. B. Schlegel, G. E. Scuseria, M. A. Robb, J. R. Cheeseman, G. Scalmani, V. Barone, G. A. Petersson, H. Nakatsuji, X. Li, M. Caricato, A. V. Marenich, J. Bloino, B. G. Janesko, R. Gomperts, B. Mennucci, H. P. Hratchian, J. V. Ortiz, A. F. Izmaylov, J. L. Sonnenberg, D. Williams-Young, F. Ding, F. Lipparini, F. Egidi, J. Goings, B. Peng, A. Petrone, T. Henderson, D. Ranasinghe, V. G. Zakrzewski, J. Gao, N. Rega, G. Zheng, W. Liang, M. Hada, M. Ehara, K. Toyota, R. Fukuda, J. Hasegawa, M. Ishida, T. Nakajima, Y. Honda, O. Kitao, H. Nakai, T. Vreven, K. Throssell, J. A. Montgomery, Jr., J. E. Peralta, F. Ogliaro, M. J. Bearpark, J. J. Heyd, E. N. Brothers, K. N. Kudin, V. N. Staroverov, T. A. Keith, R. Kobayashi, J. Normand, K. Raghavachari, A. P. Rendell, J. C. Burant, S. S. Iyengar, J. Tomasi, M. Cossi, J. M. Millam, M. Klene, C. Adamo, R. Cammi, J. W. Ochterski, R. L. Martin, K. Morokuma, O. Farkas, J. B. Foresman, and D. J. Fox, *GAUSSIAN16, revision C.01*, Gaussian, Inc., Wallingford, CT, 2016.

[95] S. Magnier, S. Rousseau, A. Allouche, G. Hadinger, and M. Aubert-Frecon, Chem. Phys. **246**, 57 (1999).

[96] H. Bouzouita, C. Ghanmi, and H. Berriche, J. Mol. Struct. Theochem. **777**, 75 (2006).

[97] P. Jasik, J. Wilczyński, and J. E. Sienkiewicz, Eur. Phys. J. Spec. Top. **144**, 85 (2007).

[98] M. Musiał, M. Medrek, and S. A. Kucharski, Mol. Phys. **113**, 2943 (2015).

[99] D. Rabli and R. McCarroll, Chem. Phys. **487**, 23 (2017).

[100] H. Berriche, Int. J. Quant. Chem. **113**, 1349 (2013).

[101] A. Bewicz, M. Musiał, and S. A. Kucharski, Mol. Phys. **115**, 2649 (2017).

[102] E. Ilyabaev and U. Kaldor, J. Chem. Phys. **98**, 7126 (1993).

[103] S. Magnier and M. Aubert-Frécon, J. Quant. Spectrosc. Radiat. Transf. **78**, 217 (2003).

[104] H. Berriche, C. Ghanmi, M. Farjallah, and H. Bouzouita, J. Comput. Methods Sci. Eng. **8**, 297 (2008).

[105] A. Jraij, A. R. Allouche, S. Magnier, and M. Aubert-Frecon, Can. J. Phys. **86**, 1409 (2008).

[106] P. Skupin, M. Musiał, and S. A. Kucharski, J. Phys. Chem. **121**, 1480 (2017).

[107] D. Rabli and R. McCarroll, Chem. Phys. Lett. **723**, 82 (2019).

[108] A. Jraij, A. Allouche, M. Korek, and M. Aubert-Frécon, Chem. Phys. **290**, 129 (2003).

[109] M. Aymar, S. Azizi, and O. Dulieu, J. Phys. B **36**, 4799 (2003).

[110] A. Jraij, A. Allouche, M. Korek, and M. Aubert-Frécon, Chem. Phys. **310**, 145 (2005).

[111] S. Magnier and M. Aubert-Frecon, J. Phys. Chem. A **105**, 165 (2001).

[112] H. Berriche, J. Mol. Struct. Theochem. **663**, 101 (2003).

[113] N. Khelifi, R. Dardouri, O. M. Al-Dossary, and B. Oujia, J. Russ. Laser Res. **30**, 172 (2009).

[114] D. Rabli and R. McCarroll, Chem. Phys. **511**, 63 (2018).
[115] H. Berriche, C. Ghanmi, and H. B. Ouada, J. Mol. Spectrosc. **230**, 161 (2005).
[116] O. M. Al-dossary and N. Khelifi, Russ. J. Phys. Chem. A **88**, 73 (2014).
[117] M. Musiał, A. Bewicz, P. Skupin, and S. A. Kucharski, Adv. Quantum Chem. **76**, 333 (2018).
[118] C. Ghanmi, M. Farjallah, and H. Berriche, Int. J. Quant. Chem. **112**, 2403 (2011).
[119] C. Ghanmi, H. Bouzouita, H. Berriche, and H. B. Ouada, J. Mol. Struct. Theochem. **777**, 81 (2006).
[120] N. Khelifi, R. Dardouri, and O. M. Al-Dossary, J. Appl. Spectrosc. **78**, 11 (2011).
[121] C. Ghanmi, H. Berriche, and H. B. Ouada, J. Mol. Spectrosc. **235**, 158 (2006).
[122] C. Ghanmi, H. Bouzouita, N. Mabrouk, and H. Berriche, J. Mol. Struct. Theochem. **808**, 1 (2007).
[123] M. Korek, K. Badreddine, and A. R. Allouche, Can. J. Phys. **86**, 1015 (2008).
[124] M. Korek, G. Younes, and A. R. Allouche, Int. J. Quant. Chem. **92**, 376 (2003).
[125] M. Korek, A. R. Allouche, and S. N. Abdul Al, Can. J. Phys. **80**, 1025 (2002).
[126] M. Korek and A. R. Allouche, J. Phys. B **34**, 3689 (2001).
[127] H. Li, H. Feng, W. Sun, Y. Zhang, Q. Fan, K. A. Peterson, Y. Xie, and H. F. S. III, Mol. Phys. **111**, 2292 (2013).
[128] N. Alharzali, D. Sardar, R. Mlika, B. Deb, and H. Berriche, J. Phys. B **51**, 195201 (2018).
[129] S. Banerjee, J. A. Montgomery, J. N. Byrd, H. H. Michels, and R. Côté, Chem. Phys. Lett. **542**, 138 (2012).
[130] P. Zhang, A. Dalgarno, and R. Côté, Phys. Rev. A **80**, 030703(R) (2009).
[131] R. ElOualhazi and H. Berriche, J. Phys. Chem. A **120**, 452 (2016).
[132] R. Bala, H. S. Nataraj, M. Abe, and M. Kajita, Mol. Phys. **117**, 712 (2019).
[133] M. Farjallah, D. Sardar, N. El-Kork, B. Deb, and H. Berriche, J. Phys. B **52**, 045201 (2019).
[134] H. Habli, L. Mejrissi, H. Ghalla, S. J. Yaghmour, B. Oujia, and F. X. Gadéa, Mol. Phys. **114**, 1568 (2016).
[135] R. Saito, S. Haze, M. Sasakawa, R. Nakai, M. Raoult, H. Da Silva, O. Dulieu, and T. Mukaiyama, Phys. Rev. A **95**, 032709 (2017).
[136] O. P. Makarov, R. Côté, H. Michels, and W. W. Smith, Phys. Rev. A **67**, 042705 (2003).
[137] M. Gacesa, J. A. Montgomery, H. H. Michels, and R. Côté, Phys. Rev. A **94**, 013407 (2016).
[138] S. Jellali, H. Habli, L. Mejrissi, R. Hamdi, B. Oujia, and F. X. Gadea, J. Quant. Spectrosc. Radiat. Transf. **209**, 45 (2018).
[139] M. Tacconi, F. A. Gianturco, and A. K. Belyaev, Phys. Chem. Chem. Phys. **13**, 19156 (2011).
[140] M. Aymar, R. Guérout, and O. Dulieu, J. Chem. Phys. **135**, 064305 (2011).
[141] S. Jellali, H. Habli, L. Mejrissi, M. Mohery, B. Oujia, and F. X. Gadea, Mol. Phys. **114**, 2910 (2016).
[142] M. Ben Hadj Ayed, R. Dardouri, H. Souissi, K. A. Alamry, B. Oujia, and F. X. Gadéa, Eur. Phys. J. D **71**, 58 (2017).
[143] S. Bellaouini, A. Pal, A. Rakshit, M. Farjallah, B. Deb, and H. Berriche, Eur. Phys. J. D **72**, 131 (2018).
[144] H. Souissi, L. Mejrissi, H. Habli, A. A. Al-Ghamdi, B. Oujia, and F. X. Gadéa, Chem. Phys. **490**, 19 (2017).
[145] S. Knecht, L. K. Soerensen, H. J. A. Jensen, T. Fleig, and C. M. Marian, J. Phys. B **43**, 055101 (2010).
[146] M. Krych, W. Skomorowski, F. Pawłowski, R. Moszynski, and Z. Idziaszek, Phys. Rev. A **83**, 032723 (2011).
[147] H. D. L. Lamb, J. F. McCann, B. M. McLaughlin, J. Goold, N. Wells, and I. Lane, Phys. Rev. A **86**, 022716 (2012).
[148] E. R. Sayfutyarova, A. A. Buchachenko, S. A. Yakovleva, and A. K. Belyaev, Phys. Rev. A **87**, 052717 (2013).
[149] M. Tomza, Phys. Rev. A **92**, 062701 (2015).
[150] J. Deiglmayr, M. Aymar, R. Wester, M. Weidemuller, and O. Dulieu, J. Chem. Phys. **129**, 064309 (2008).
[151] See Supplemental Material at http://link.aps.org/supplemental/10.1103/PhysRevA.101.012501 for a detailed comparison of the calculated spectroscopic parameters for the diatomic molecular ions presented in the main text with the previous calculations and measurements.
[152] F. Wang and E. I. von Nagy-Felsobuki, Theor. Chem. Acc **88**, 131 (1994).